Student thesis

NTNU
Norwegian University of Science and Technology
Faculty of Engineering
Department of Energy and Process Engineering

Leire Juaristi

An experimental study of the performance of a wind turbine model with swept blades, for different inflow conditions

Student thesis in Master
Supervisor: Tania Bracchi
June 2023

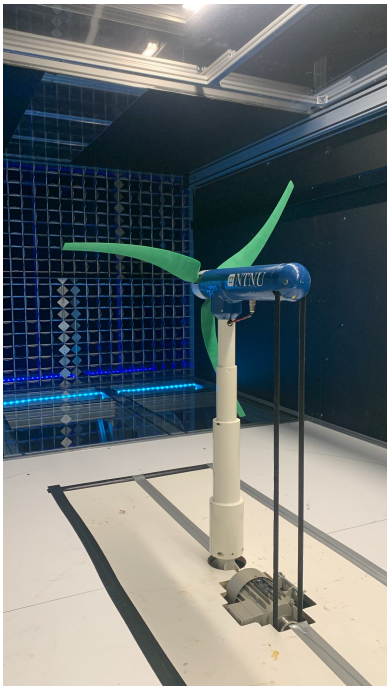

NTNU
Norwegian University of
Science and Technology

Leire Juaristi

An experimental study of the performance of a wind turbine model with swept blades, for different inflow conditions

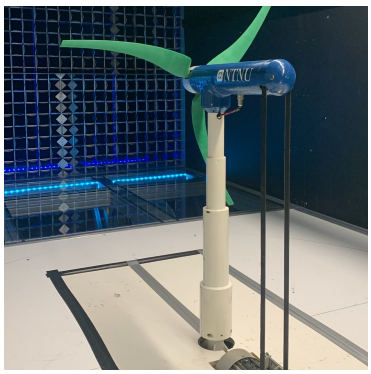

Student thesis in Master
Supervisor: Tania Bracchi
June 2023

Norwegian University of Science and Technology
Faculty of Engineering
Department of Energy and Process Engineering

NTNU
Norwegian University of
Science and Technology

Leire Juaristi

An experimental study of the performance of a wind turbine model with swept blades, for different inflow conditions

Master's thesis in Thermo- and Fluid Dynamics

Faculty of Engineering

Department of Energy and Process Engineering

Supervisor: Tania Bracchi

June 2023

Acknowledgements

I would like to express my deepest gratitude to my master's thesis supervisor, Tania Bracchi, for her invaluable guidance, support, and expertise throughout the entire process. Also for giving me the opportunity to do this thesis in their department and facilitating the acceptance and adaptation process. I am also indebted to the faculty members of Energy and Process Engineering department at NTNU for their knowledge, inspiration, and encouragement. I would like to extend my appreciation to the participants who willingly took part in this study. I am also thankful to my family and friends, specially my friends in Trondheim, for their unwavering support, encouragement, and understanding throughout this academic journey. Furthermore, I would like to thank my partner for encouraging me to venture into this experience from the very beginning and for always believing in me. Their love, patience, and belief in my abilities have been a constant source of motivation. Finally, I would like to express my gratitude to all those who have contributed in any way to this thesis, directly or indirectly.

Abstract

This Master Thesis is the continuation of Tarald's Master Thesis (year 2021), repeating the same calculations with the same models already created, but extending the sampling time.

An experimental investigation was conducted in a wind tunnel to analyze the aerodynamic performance of a horizontal axis wind turbine model equipped with forward and backward swept blades. An active grid produced homogeneous, isotropic, freestream turbulence with assumed turbulence intensities of 3%, 8%, and 13%. Already manufactured three distinct wind turbine models were used, all made by a polyurethane base material, each with a rotor diameter of 0.9 meters: straight blades like a baseline model to isolate the effect of blade sweep, and the two models with swept blades, introducing a pre-bending of the straight wind turbine blades in the rotational plane. The two swept blades were identical except for the blade sweep direction, either forward or backward swept relative to the rotation of the rotors. The experimental results indicate that, under the tested conditions, the wind turbine model with straight blades consistently outperformed both the forward and backward swept blade configurations. However, this superiority was observed only when the wind turbine models were tested without an active grid installed. In medium turbulence intensity, the forward swept blades had a 13.56 % lower maximum power coefficient at the expense of an decrease in the thrust coefficient of 6.71%. The backward swept blades experienced a 15.68 % lower maximum power coefficient and a further decrease in the thrust coefficient of 13.74 % compared to the straight blades. Nevertheless, in high turbulence intensity, the forward swept blades had a 4.96 % lower maximum power coefficient at the expense of an decrease in the thrust coefficient of 0.68%. The backward swept blades experienced a 9.72% lower maximum power coefficient and a further decrease in the thrust coefficient of 10.28% compared to the straight blades.

KEYWORDS:

Wind turbine, power coefficiente, C_P, thrust coefficient, C_T, wind speed, turbulence, stright blades, forward swept blades, backward swept blades.

Sammendrag

Denne masteroppgaven er en fortsettelse av Taralds masteroppgave (år 2021), som gjentar de samme beregningene med de samme modellene som allerede er opprettet, men forlenger prøvetakingstiden.

En eksperimentell undersøkelse ble utført i en vindtunnel for å analysere den aerodynamiske ytelsen til en vindturbinmodell med horisontal akse utstyrt med forover- og bakoversveide blader. Et aktivt rutenett produserte homogen, isotrop, fristrømsturbulens med antatte turbulensintensiteter på 3 %, 8 % og 13 %. Allerede produserte tre forskjellige vindturbinmodeller ble brukt, alle laget av et polyuretanbasemateriale, hver med en rotordiameter på 0,9 meter: rette blader som en grunnlinjemodell for å isolere effekten av bladsveip, og de to modellene med feide blader, introduserer en forbøyning av de rette vindturbinbladene i rotasjonsplanet. De to feide bladene var identiske bortsett fra bladsveiperetningen, enten forover eller bakover sveipet i forhold til rotasjonen til rotorene. De eksperimentelle resultatene indikerer at vindturbinmodellen med rette blader under de testede forholdene konsekvent overgikk både de forover og bakover feide bladkonfigurasjonene. Denne overlegenheten ble imidlertid kun observert når vindturbinmodellene ble testet uten installert et aktivt nett. I middels turbulensintensitet hadde de foroversveide bladene en 13,56 % lavere maksimal effektkoeffisient på bekostning av en reduksjon i skyvekraftskoeffisienten på 6,71 %. De bakover feide bladene opplevde en 15,68 % lavere maksimal effektkoeffisient og en ytterligere reduksjon i skyvekraftskoeffisienten på 13,74 % sammenlignet med de rette bladene. Ikke desto mindre, i høy turbulensintensitet, hadde de foroversveide bladene en 4,96 % lavere maksimal effektkoeffisient på bekostning av en reduksjon i skyvekraftskoeffisienten på 0,68 %. De bakover feide bladene opplevde en 9,72 % lavere maksimal effektkoeffisient og en ytterligere reduksjon i skyvekraftskoeffisienten på 10,28 % sammenlignet med de rette bladene.

Preface

This Master's Thesis was written at the Norwegian University of Science and Technology (NTNU), Department of Energy and Process Engineering (EPT), Fluid Mechanics Laboratory. The analysis and written paper began in early March 2023, and laboratory tests were performed in late April, between the 24th of April and 6th of May. The thesis is presented in paper format as a research article. The template suggested by the NTNU has been used as a basis. The suggested index and points are followed, adapting to the topic, and adding appendices with additional information, relevant for the Master's thesis. Initially, the laboratory tests were going to be carried out at the beginning of the project, first of March, but since the laboratory was not ready, the planning had to be restructured.

Problem description and goals

Numerous studies have been conducted on swept blades, examining their aerodynamic behavior and performance in both large-scale MW-scale wind turbines and small-scale wind turbines, as described in chapter 1.3. However, despite the existing body of research, there is still a need for further investigation into the aerodynamics of rotor systems equipped with swept blades. In the current study, taking as a basis Tarald's Master's Thesis, a wind turbine model provided by NTNU (Norwegian University of Science and Technology) with straight blades will serve as the reference or baseline model for the investigation of swept blade designs. Using the NTNU wind turbine model with straight blades as a baseline allows for a comparative analysis of the performance of the swept blade configurations. The study will focus on comparing the performances and loads of two different rotors.

The goals of the project are:

- Improve the results of a previous study, increasing the sampling time,
- Measure power and thrust for different TSR (Tip Speed Ratio),
- Measure the wake for different TSR.

The following tasks are to be considered:

- Tarald's Master's Thesis, 2021, since the present thesis is the continuation of the previous one, increasing the sampling time,
- Perform a detailed literature review on horizontal axis wind turbines with swept blades,
- Get familiar with the experimental setup in the wind tunnel and the data acquisition,
- Analyze the results and make conclusions.

Table of Contents

List of Figures

List of Tables

List of Abbreviations

NTNU	The Norwegian University of Science and Technology
WT	Wind Turbine
SI	International System of Units
TSR	Tip Speed Ratio
Cp	Power coefficient
Ct	Thrust coefficient
P	Power
S	Straight blades
F	Forward swept blades
B	Backward swept blades

1 INTRODUCTION

1.1 Energy context

1.1.1 Energy

The definition of energy (The Editors of Encyclopaedia Britannica, n.d.), according to physics, is the capacity for doing work, existing in different forms like: kinetic, potential, thermal, electrical, nuclear, chemical… In the International System of Units (SI), energy is measured in joules (J).

As demonstrated by the principle of conservation of energy or the first law of thermodynamics, Energy cannot be created or destroyed, only changed from one form to another. It is possible to convert energy from one form to another in several ways. For example, usable mechanical or electrical energy can be produced by different types of devices, such as generators, heat engines, batteries, fuel cells, and magnetohydrodynamic systems.

1.1.2 Situation today

To ensure that everyone in the world has access to clean and safe energy, it must be understood today's energy consumption, its evolution, and its impacts around the world. Figure 1 shows the energy use per person around the world in 2021 (Hannah Ritchie, Max Roser and Pablo Rosado, 2022). The terms "energy" and "electricity" are not the same concept, since electricity is only one component of total energy consumption. The concept of of *Energy use* includes electricity, transport, heating and cooking.

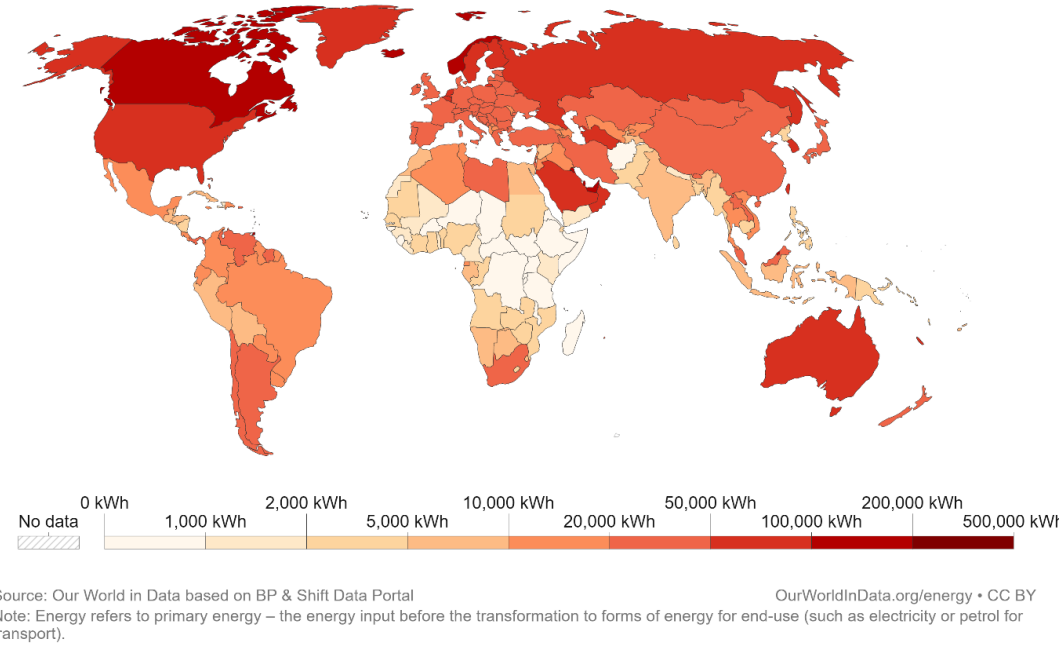

Figure 1. Energy use per person 2021.

Figure 2 presents the evolution of the energy use per person since 1965 until 2021, in Norway, Europe and average of the world.

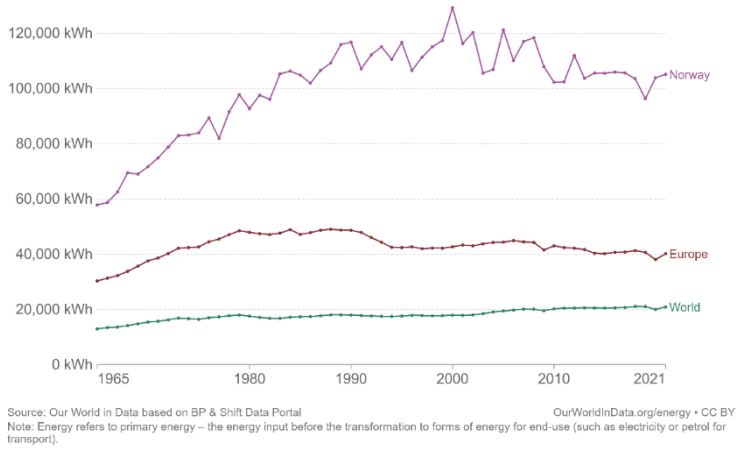

Figure 2. Evolution of the energy use per person in Norway, Europe and World.

Three different trends are perceived:

- World: consumption has been increasing little by little, from a total of 15,000 kWh to about 21,000 kWh.
- Europe: there was a significant rise in the 80s, and since the 90s it has been stabilizing around 40,000 kWh.
- Norway: many peaks. Overall, since the 1960s, energy use has increased by more than 70%. It should be noted that around the year 2000 the initial consumption was doubled.

Today, the world does not have safe, low-carbon, and cheap large-scale energy alternatives to fossil fuels.

Therefore, until they are achieved, the world faces the following problems: hundreds of millions of people lack access to sufficient energy, and the dominance of fossil fuels in energy system drives climate change and health impacts (air pollution). Then, it is evident that the production of energy, especially the burning of fossil fuels and biomass, drives three quarters of the generation of greenhouse gas emissions and influence in human health, creating five million deaths due to air pollution.

Energy mix (Hannah Ritchie and Max Roser, 2022) gives the view of the global primary energy consumption by source, during last sixty years (Figure 4):

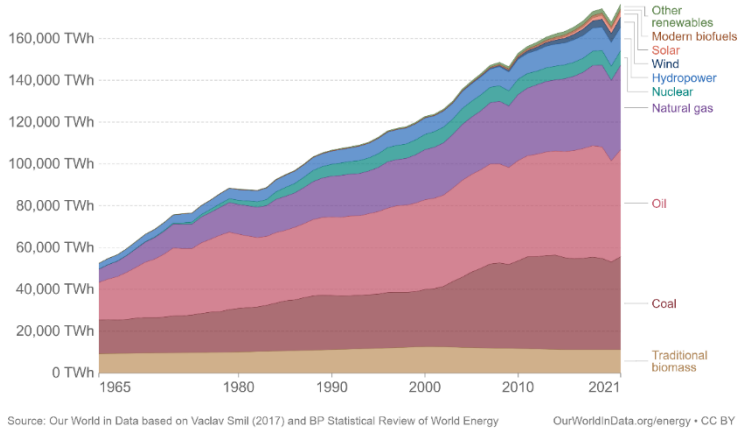

Figure 4. Global primary energy consumption by source 1965-2021.

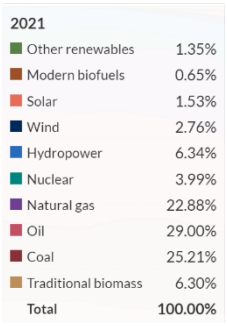

Figure 3. Relative % of global primary energy consumption by source, 2021.

According to the latest data found, from the year 2021, Figure 3 shows the relative percentage of world primary energy consumption by source. There can be seen that almost Natural gas, Oil and Coal are the most used still, followed by hydropower and traditional biomass. Wind energy joined with 2.76 %.

Moreover, the case of Norway changes (Figure 5 and Figure 6):

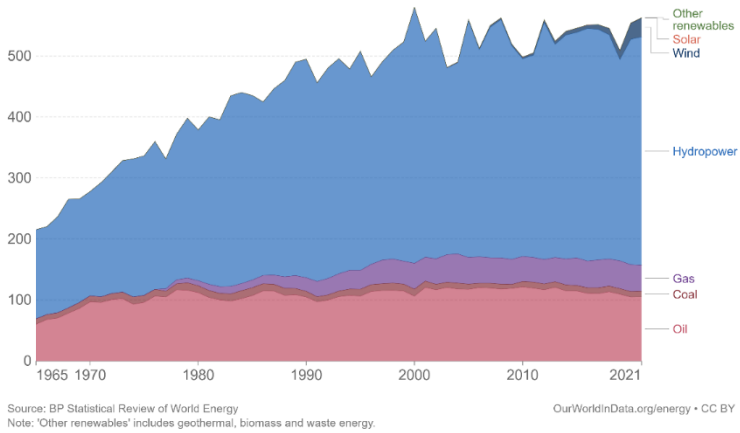

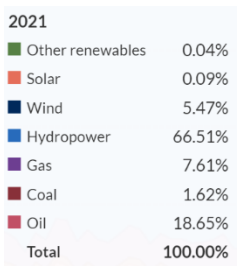

Figure 5. Relative % of Energy consumption by source, Norway, 2021.

Figure 6. Energy consumption by source in TWh, Norway, 1965-2021.

In the last 50 years, energy consumption by coal and oil has remained more or less constant, when gas increased in the 1990s, and hydropower has been growing over the years, presenting peaks every two years. Hydropower is Norway's great source of energy.

When analyzing the generation of electricity, we are focusing on the annual average electricity generation per person in each country (kWh).

In this case, focusing on Europe, it can be seen (Figure 7) that Norway, Sweden and Iceland are the three countries that generate the most electricity per capita last year.

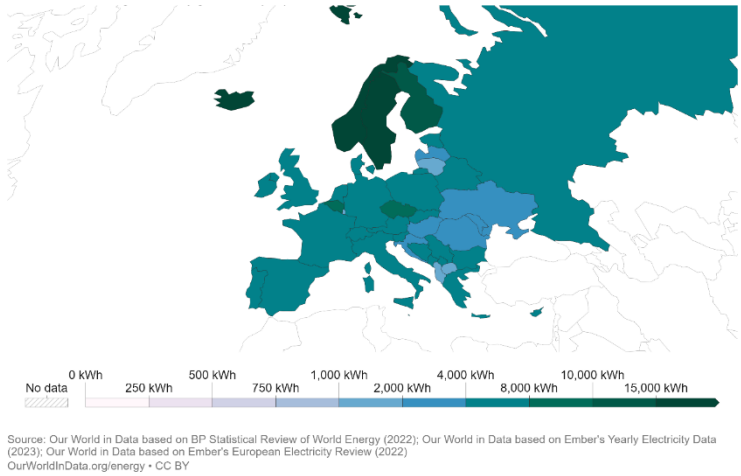

Figure 7. Per capita electricity generation 2022.

Nevertheless, since this document deals with wind turbines, the situation of wind energy at a global and Norwegian level is briefly described.

1.2 Wind energy

1.2.1 Wind power generation

To talk about wind energy (Hannah Ritchie, Max Roser and Pablo Rosado, 2022), we will first place it within renewable energy. World data from 2021 (Figure 8) show that the more used renewable energy was hydropower, followed by win energy and solar energy. The same trend occurs in Norway, but the difference between hydropower and wind energy (Figure 9).

2021	
Other renewables	9.62%
Solar	13.02%
Wind	23.48%
Hydropower	53.89%
Total	**100.00%**

Figure 8. Relative % of renewable energy generation, World, 2021.

2021	
Other renewables	0.16%
Solar	0.13%
Wind	7.58%
Hydropower	92.13%
Total	100.00%

Figure 9. Relative % of renewable energy generation, Norway, 2021.

Now focising in the Wind Energy, World and Norwegian data will be compared.

Annual electricity generation coming from wind energy includes both onshore and offshore wind sources and it is measured in TWh/year.

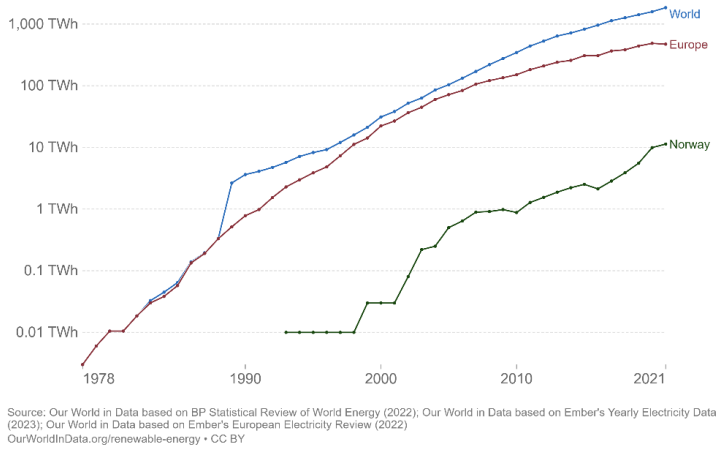

Figure 10. Wind energy generation in the World, Europe and Norway during last 40 years.

1.2.2 Installed wind capacity

Power generation is a function of how much wind capacity is installed (Hannah Ritchie, Max Roser and Pablo Rosado, 2022). Figure 11 shows installed wind capacity, both onshore and offshore, around the World, Europe and Norway, measured in GW. Energy output is a function of power (installed capacity) multiplied by the time of generation.

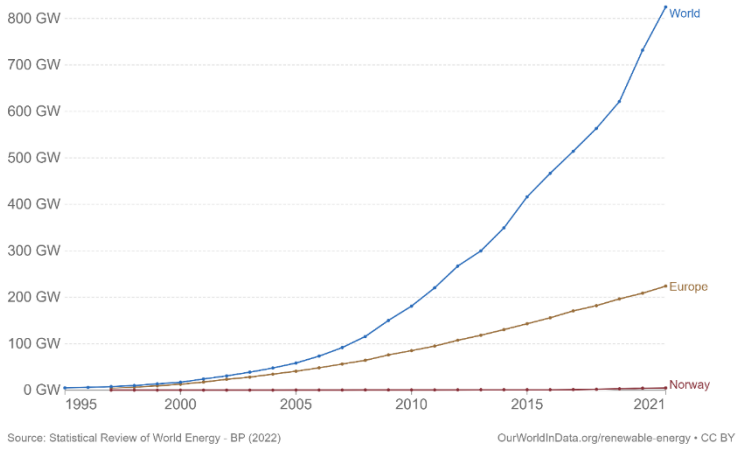

Figure 11. Installed wind energy capacity, in the World, Europe and Norway.

1.2.3 Wind in the energy and electricity mix

In 2021, around 2.95 % of global energy came from wind (Hannah Ritchie, Max Roser and Pablo Rosado, 2022). According to Figure 12, wind energy began to be used in the 2000s, in the world and Europe it had a more progressive rise than in Norway.

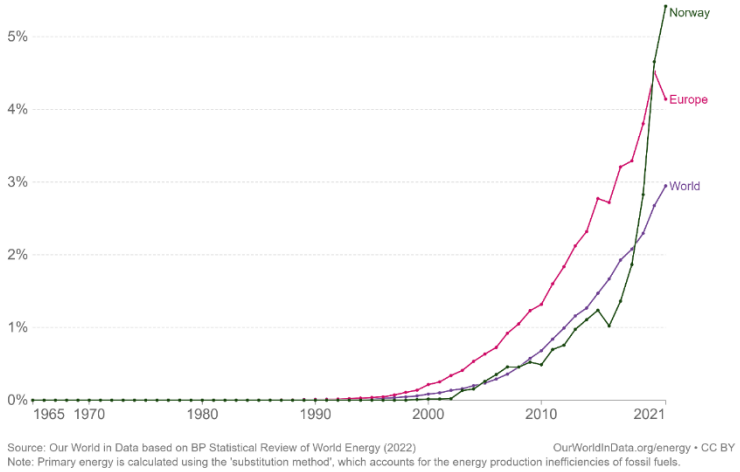

Figure 12. Share of primary energy from wind, in the World, Europe and Norway.

In the world it has risen by 15% per year. In Europe a 10 % growth until 2010 and then 30%, until having a decrease from 2020 to 2021. And in Norway, the big rise was seen from 2016 to 2021.

From that power generation, the share of electricity that comes from wind in the last year analyzed was (Hannah Ritchie, Max Roser and Pablo Rosado, 2022): 6.65 % in the world, 9.91 % in Europe and 7.49 % in Norway.

1.3 Different studies

After analizing a bit the evolution of the energy context during the last sixty years, and focusing in Renewable enegy, wind and solar sources are growing quickly (Hannah Ritchie and Max Roser, 2022). For this, in search of a transition towards a more sustainable future and a production of renewable and clean energy, it is

very important to continue researching and working on new, more efficient technologies. The goal of wind turbines *(from now on also called WT)* is to use the kinetic energy of the wind to generate electricity. To do this, the wind blows the turbine blades attached to a rotor and the rotor spins a generator that creates electricity. Nowadays, there are two typical types of wind turbines: the horizontal-axis wind turbines, also known as HAWTs, and vertical-axis wind turbines, VAWTs (National Geographic, 2022). However, the most common are HAWTs with three long, thin blades positioned to face directly into the wind. On the other hand, VAWTs have shorter and greater curved blades.

The manufacture of rotors with larger diameter has significantly increased the total power of wind turbines (G.M. Joselin Herbert, S. Iniyan, E. Sreevalsan, S. Rajapandian, 2007), and to that must be added innovations in the design of the rotor blades, for greater efficiency. Obviously, larger rotor diameters mean higher maintenance costs and shorter life expectancy. Therefore, with the aim of reducing costs and increasing the life expectancy of turbines, increasing aerodynamic efficiency and reducing loads on the blades must be studied.

Wind turbine blades use airfoils to develop mechanical power (J.F. Manwell, J.G. McGowan and A.L. Rogers, 2002) and the cross-sections of wind turbine blades have the shape of airfoils. The width and length of the blade are functions of the desired aerodynamic performance, the maximum desired rotor power, the assumed airfoil properties and strength consideration. There are many types of airfoils, and new airfoils have significantly increased the aerodynamic efficiency of wind turbines (Office of Geothermal and Wind Technologies, 2000). Researchers have always attempted to use airfoils with high aerodynamic efficiency in blade design (Vahid Akbari, Mohammad Naghashzadegan, Ramin Kouhikamali, Farhad Afsharpanah and Wahiba Yaïci, 2022). Generally, in the case of large turbines, several airfoils are used on different parts of the blades, each with its own task.Thin airfoils (Figure 13) with better aerodynamic performance are used at the tip of the blade to provide more power, while thick airfoils (Figure 13) are used at the root of large blades to resist structural stresses.

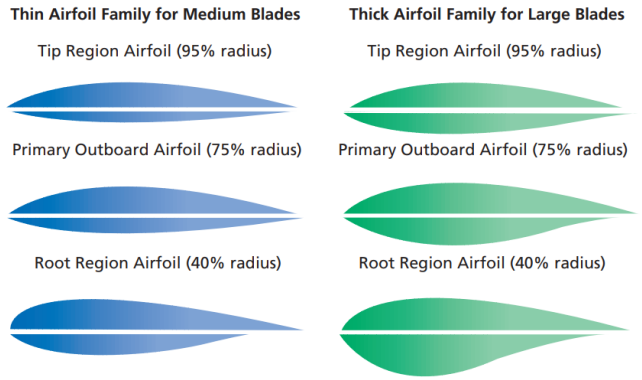

Figure 13. Types of thin and thick airfoil families.

As the type of aerodynamic profile used in the blade is very important for the aerodynamic performance of a wind turbine, its proper selection needs additional

study, regarding the starting process. As mentioned above, horizontal axis turbines are the most common, and their blades can be found in many different shapes and forms.

Several studies have been performed on horizontal axis wind turbines with swept blades, also in the NTNU (Tarald Wærness, 2021). Still today, the most complete study that exists on this subject is: The development of the Sweep-Twist Adaptive Rotor (STAR) by Knight & Carver Wind Group and Sandia National Laboratories (Ashwill T, Kanaby G, Jackson K, Zuteck M, 2010). The project consisted on a design and fabrication of a 27.1 m STAR blade, static and fatigue laboratory tests, esting on a Zond 750 test turbine, where wind speeds average around 5.8 m/s. As a result, the STAR shovel exceeded the project's stated target (annual energy capture improvement over baseline) and produced 10-12% more energy.

In the analysis of aerodynamics of wind turbines, details of momentum theory and blade element theory are developed and used to calculate the optimum blade shape for simplified and ideal conditions (J.F. Manwell, J.G. McGowan and A.L. Rogers, 2002). The combination of the two approaches, called strip theory or blade element momentum (BEM) theory, is used to outline a procedure for the aerodynamic design and performance analysis of a wind turbine rotor. Although most recent studies on swept blades utilize the well-established BEM method, the analysis of aerodynamic design is not the objective of this document, but some studies will be mentioned. In the article *A computationally efficient engineering aerodynamic model for swept wind turbine blades* (Ang Li, Georg Raimund Pirrung, Mac Gaunaa, Helge Aagaard Madsen, and Sergio González Horcas, 2022), a model for the extended blade element moment (BEM) formulation is proposed. It is concluded that the far and near wake model is combined with a coupling factor, making the thrust of the entire rotor similar to that calculated with BEM method, because it is based on a far-wake BEM method. It is shown that, according to the numerical comparison, the BEM method is not capable of correctly modeling the influence of the blade sweep and has great differences with the results of the more fidelity models. Therefore, the improvement of the coupled method proposed in the article is significant, and there are several future works to further improve the model.

In the search and analysis of ways to increase annual energy production (AEP) in recent years, there are studies of extending the length of the installed blades, joining a longer blade piece to the real tip, solutions such as increasing the rotor diameter (Enel Green Power, 2022). The following study (Liz Hartman, 2022) shows that Wind Turbines, the bigger the better, in other words, while the diameter of the rotor is greater, and with it the height of the hub (distance from the ground to the middle of the turbine’s rotor) is higher, the production capacity increases (Figure 14).

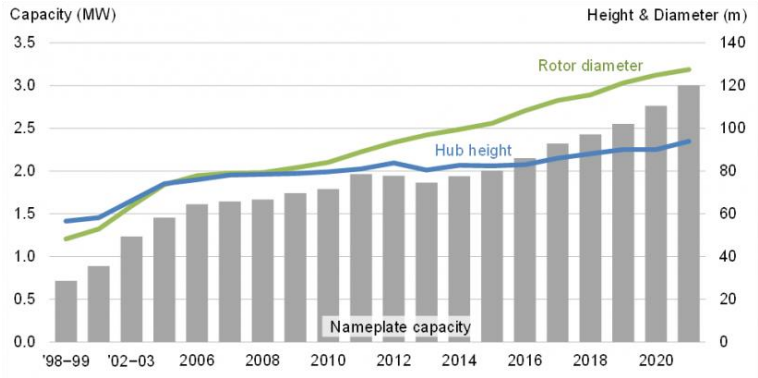

Figure 14. Average turbine hub height, rotor diameter, and nameplate capacity for land-based wind projects.

The hub height for onshore has increased 66% since 1998, about 94 m in 2021; and the avergae of offshore hub height will increase from 100 m in 2016 to 150 m in 2035. About the rotor diamenter, has also grown over the years, in 2021 the avergae was 127.5 m, this makes rotor swept areas have grown around 600 % since 1998. The capacity of recently installed WTs in 2021 is 319 % higher than in 1998.

However, as the present study deals with swept blades, will focus on the difference in annual energy production between swept and stright blades. Based on the results of this recent study (Xiaoxi Huang, Junwei Yang, Zhiying Gao, Chenglong Sha and Hua Yang, 2022), swept blades had a 1.34% increase in maximum AEP compared to reference straight blades, while also having a reduction in blade root load, assuming a decrease in the cost of the wind turbine. Even so, another older study analized the design of swept blades to increase AEP 5 % over the straight blade, without increasing blade loads (Scott Larwood, C.P. van Dam and Daniel Schow, 2014).

A recent study explores the Output Power and Wake Flow Characteristics of a Wind Turbine with forward and backward Swept Blades (Xiaoxi Huang, Junwei Yang, Zhiying Gao, Chenglong Sha and Hua Yang , 2022). The results indicate that for both forward and backward swept blades (at yaw angles of 0°, 10°, 20°, and 30°), increasing the blade tip offset and the sweep start location could decrease the power and thrust coefficients. The forward swept design significantly improved the blades' power characteristics, compared to the backward swept one. Using swept blades instead of straight blades, as the tip speed ratio increased to a larger value, WTs could generate more power at high tip speed ratios, especially in yaw conditions.

This project aims to fill a research gap identified in the literature by conducting an experimental study on wind turbines under varying turbulence levels. Despite numerous studies in the field, there is a notable lack of experimental investigations specifically examining the effects of different turbulence intensities on the aerodynamic performance of wind turbines. By addressing this gap, the present study aims to provide valuable insights into the impact of turbulence on power

production and blade forces, explaining and clarifying the behavior of wind turbines in realistic operating conditions.

Therefore, in 2021 a study was carried out in the NTNU wind tunnel, combining swept blades with different levels of turbulence, carried out by Tarald Wærness. In that project, the results obtained were not accurate. That is, the resulting curves exhibited jagged or spiky characteristics, limiting the reliability and interpretability of the data. In order to address this limitation and ensure more accurate measurements, a longer sampling time was deemed necessary to allow for proper flow convergence. In Tarald's thesis sampling time was thirty seconds, while in this present thesis, the sampling times are: two minutes for the cases of non-turbulence and low turbulence, and six minutes for those of medium and high turbulence intensity. By doing so, the thesis aimed to obtain smoother and more reliable curves, facilitating a more comprehensive analysis of the turbulent cases.

1.4 Atmospheric turbulence

The wind speed suffers variations in time by the following categories: inter-annual, annual, diurnal and short-term (gusts and turbulence) (J.F. Manwell, J.G. McGowan and A.L. Rogers, 2002). Short-term variations are generally ten minutes or less. Variations in wind speed with periods of less than 1 second to 10 minutes and that have a stochastic character are considered representative of turbulence, and for wind power applications, it is necessary to quantify the turbulent fluctuations in the flow.

As a definition, turbulence can be considered a random fluctuation of wind speed imposed on the average wind speed, occurred in three directions: longitudinal (direction of the wind), lateral (perpendicular to the average wind), and vertical. It is originated by the dissipation of the kinetic energy of the wind into thermal energy with the creation and destruction of progressively smaller eddies or gusts. Turbulent wind may be quite variable in short times (minutes or less) but may have a constant mean in longer periods (an hour or more). Although wind variability appears to be quite random on the surface, it actually has characteristics with the following statistical properties:

- turbulence intensity
- wind speed probability density function
- autocorrelation
- integral time scale/length scale
- power spectral density function.

The intensity of the turbulence (the most basic measure of turbulence) is defined by: the ratio between the standard deviation of the wind speed and the mean wind speed. The length of the time period that calculates both the mean and standard deviation is normally no more than 1 hour, and equal to 10 minutes in wind energy engineering.

The turbulence intensity, TI:

$$TI = \frac{\sigma_u}{U} \qquad \textbf{(1)}$$

Where,

σ_u= standard deviation

$$\sigma_u = \sqrt{\frac{1}{N_S - 1}\sum_{i=1}^{N_S}(u_i - U)^2} \qquad \textbf{(2)}$$

The usual turbulence intensity is between 0.1 to 0.4 and generally, the highest turbulence intensities occur when the wind speed is the lowest, depending the lower limiting value on the specific terrain features and surface conditions at the site.

The effect of turbulence causes the actual wind speed at any location also varies in time and direction around its due mean value. The Figure 15 clearly shows that the mean wind speed increases with height, defining the wind shear phenomenon.

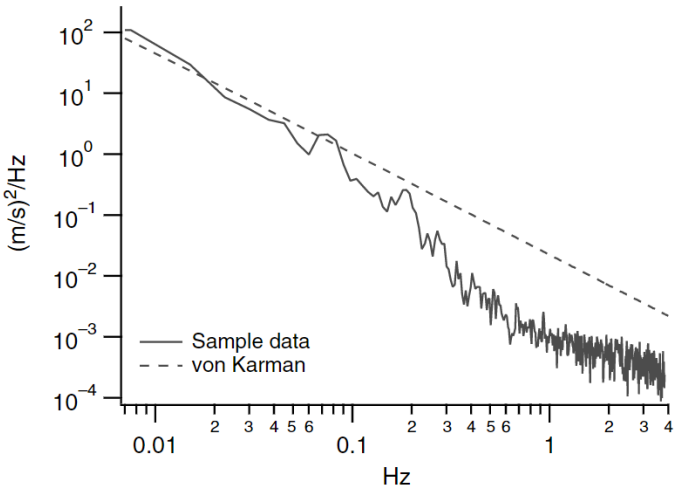

Figure 15. Wind data power spectral density functions.

1.4.1 Analysis and Characterization of Wind Turbulence

Turbulence causes: random and fluctuating loads and output power, stresses throughout the turbine structure and in the tower, therefore, knowledge of the fundamentals of turbulence is important (J.F. Manwell, J.G. McGowan and A.L. Rogers, 2002).

Ultimately, turbulence should be considered for the following purposes: maximum load prediction, structural excitation, fatigue, control and power quality. Although turbulence is a complicated subject to study, several advances have been made in wind energy engineering. For example, Figure 16 shows the turbulence characterization scheme used by NREL for their 'combined experiment' test program, consisted of a plane array of 13 anemometers used to measure the wind inflow. This system takes very little time to collect large amounts of data.

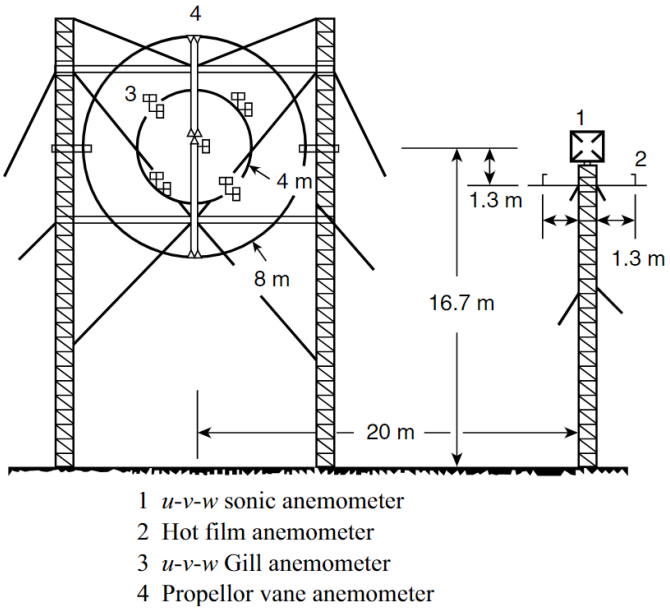

Figure 16. National Renewable Energy Laboratory combined experiment anemometry system (Butterfield, 1989).

1.5 Parameters characterizing a wind turbine

This chapter focuses on the characterization of wind turbines using non-dimensional parameters to analyze their power production and the aerodynamic forces exerted on the blades. These non-dimensional parameters provide valuable insights into the performance and behavior of wind turbines, enabling researchers to evaluate and compare different designs and operating conditions.

1.5.1 Power coefficient

Wind turbine rotor performance is usually characterized by its power coefficient, C_P (J.F. Manwell, J.G. McGowan and A.L. Rogers, 2002).

$$C_P = \frac{P}{\frac{1}{2}\rho U^3 A} = \frac{Rotor\ power}{Power\ in\ the\ wind} \qquad \textbf{(3)}$$

Where,

ρ = the air density,

U= wind speed,

$A = \pi r^2$, the total sweep area of the rotor,

The non-dimensional power coefficient represents the fraction of the power in the wind that isextracted by the rotor.

To know the maximum C_P, the following equation must be analyzed:

$$C_P = 4a(1-a)^2 \qquad \textbf{(4)}$$

Where,

a= the axial induction factor.

Then, its maximum is determined by taking the derivative of the power coefficient with respect to a and setting it equal to zero, yielding a=1/3.

$$C_{P,max} = 16/27 = 0.5926$$

$C_{P,max}$, also known as Betz limit, is the maximum theoretically possible rotor power coefficient.

This case (a= 1/3), shows that if an ideal rotor were designed and operated such that the wind speed at the rotor were 2/3 of the free stream wind speed, then it would be operating at the point of maximum power production (J.F. Manwell, J.G. McGowan and A.L. Rogers, 2002). Besides, this is the maximum power possible.

Typically, the power coefficient initially increases with increasing wind speed, as the turbine captures more energy from the wind. There is a specific wind speed, known as the rated wind speed, at which the power coefficient reaches its maximum value. Beyond the rated wind speed, the power coefficient tends to decrease due to the limitations of the turbine's design and operation.

1.5.2 Thrust coefficient

The thrust on a wind turbine can be characterized by a non-dimensional thrust coefficient (J.F. Manwell, J.G. McGowan and A.L. Rogers, 2002),

$$C_T = \frac{T}{\frac{1}{2}\rho U^2 A} = \frac{Thrust\ force}{Dynamic\ force} \qquad \textbf{(5)}$$

Where,

F_T= the total thrust force acting on the rotor,

ρ = the air density,

U= wind speed,

$A = \pi r^2$, the total sweep area of the rotor,

To know the C_T for an ideal wind turbine, it is needed the axial thrust on the disc:

$$T = \frac{1}{2}\ \rho U^2 A[4a(1-a)] \qquad \textbf{(6)}$$

And then, the thrust coefficient for an ideal wind turbine is equal to 4a(1-a).

$C_{T,max} = 1$ when, a= 0.5 and downstream velocity=0

$C_{T,max} = 8/9$ when, a= 1/3 (maximum power output)

The idealized model is not valid for axial induction factors bigger than 0.5. In the reality, complicated flow patterns not represented in this model result in thrust coefficients that can be as high as 2.0. It is important to note that the ideal thrust coefficient value depends on various factors, including the specific design and operating conditions of the wind turbine. In certain scenarios, such as in wind farms or regions with limited space, a lower thrust coefficient may be preferred to minimize wake effects and optimize the overall efficiency of the wind turbine array. However, a high thrust coefficient can be advantageous because it indicates that

the wind turbine is effectively converting a larger portion of the incoming wind's kinetic energy into thrust force. This can result in increased power generation and improved overall performance of the wind turbine. Higher thrust coefficients are often associated with greater power extraction capabilities, which can be beneficial for maximizing energy production.

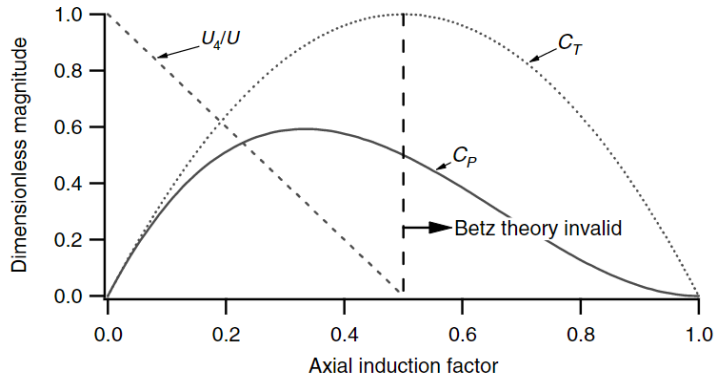

Figure 17. A graph of the power and thrust coefficients foran ideal Betz turbine and the non-dimensionalized downstream wind speed.

1.5.3 The tip speed ratio

It is defined as the ratio of the blade tip speed to the free stream wind speed (J.F. Manwell, J.G. McGowan and A.L. Rogers, 2002),

$$\lambda = \frac{\omega R}{U} \qquad \textbf{(7)}$$

Where,

ω = the angular velocity of the rotor,

R = the radius of the blades,

U= wind speed.

The results of the Figure 18 show that the higher the tip speed ratio is, the closer the C_P can approach the theoretical maximum value.

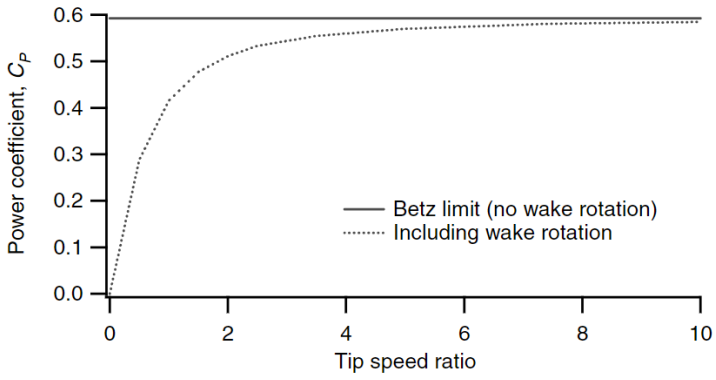

Figure 18. Theoretical maximum power coefficient as a function of tip speed ratio for an ideal horizontal axis wind turbine, with and without wake rotation.

1.6 Relative velocity (U_{rel})

To introduce the concept of relative velocity (U_{rel}) Figure 19 and Figure 20 are essential. It is a critical parameter in determining the aerodynamic performance and power generation of the wind turbine.

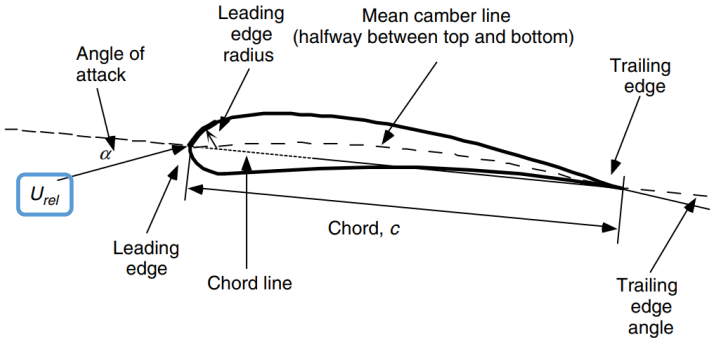

Figure 19. Airfoil nomenclature.

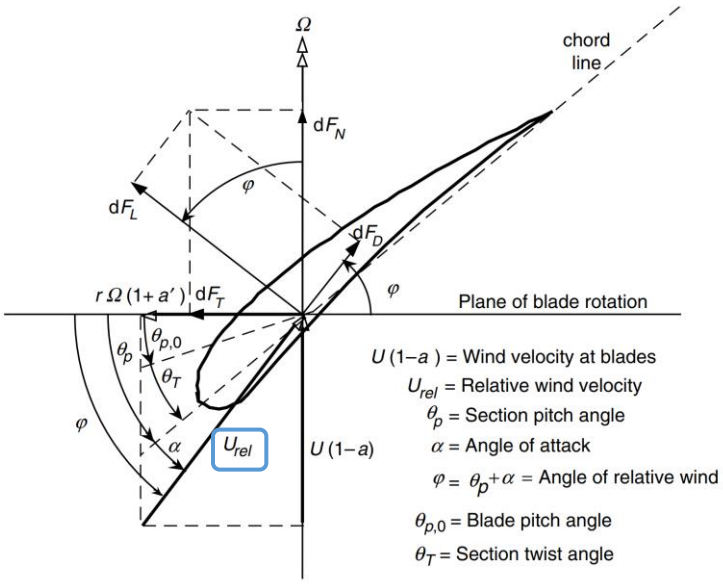

Figure 20. Blade geometry for analysis of a horizontal axis wind turbine (J.F. Manwell, J.G. McGowan and A.L. Rogers, 2002).

It is calculated by subtracting the velocity of the wind turbine's rotation from the freestream wind velocity. It represents the effective wind speed experienced by the rotor blades, taking into account the rotational motion of the blades. The magnitude and direction of Urel affect the angle of attack of the blades and the resulting lift and drag coefficients. These coefficients, in turn, determine the amount of power that can be extracted from the wind by the turbine. In wind turbines, the goal is to maximize the energy capture from the wind, which is achieved by optimizing the angle of attack of the blades based on the relative wind velocity U_{rel}. It is is limited to the free stream velocity:

$$U_{rel} = U(1-\lambda)\,\lambda < 1 \qquad \textbf{(8)}$$

From Figure 20:

$$U_{rel} = U(1 - \mathrm{a})/\sin\varphi = \frac{2U}{3\sin\varphi} \qquad \textbf{(9)}$$

1.7 Reynolds number

The Reynolds number is a no-dimensional quantity used to characterize the flow regime and determine the significance of viscous effects in fluid flow. It is defined as the ratio of inertial forces to viscous forces and is commonly used in aerodynamics to study the behavior of fluids around objects like wind turbine blades. The dependence is significant because the flow conditions in wind tunnel experiments, where the Reynolds numbers are typically lower than those in full-scale wind turbines, may differ from real-world operating conditions. By studying the dependance, information can be obtained on how aerodynamic characteristics such as power output, thrust and efficiency are influenced by changes in the flow regime. Mathematically, it is expressed as:

$$Re = \frac{\rho\, U_{rel}\, \mathrm{c}}{\mu} \qquad \textbf{(10)}$$

Where,

ρ = is the density of the fluid,

U_{rel} = is the relative velocity,

c = is the chord length of the airfoil,

μ = is the dynamic viscosity of the fluid.

Indeed, the performance of a model wind turbine is highly dependent on the Reynolds number (Re), which is closely related to the freestream velocity (U). The freestream velocity, U, represents the speed of the incoming wind that interacts with the turbine blades. As the freestream velocity increases, the Reynolds number also increases, resulting in a transition from laminar to turbulent flow. At lower Reynolds numbers, laminar flow, the boundary layer remains relatively thin, and flow separation is less likely to occur. In this regime, the turbine may exhibit smoother airflow, lower drag, and more predictable performance characteristics. However, as the Reynolds number increases and the flow becomes turbulent, the boundary layer thickens, and flow separation becomes more prominent. Turbulent flow can introduce higher drag forces and potentially affect the turbine's efficiency and power output.

While the performance of a wind turbine is generally influenced by the freestream velocity and Reynolds number, there is a threshold beyond which the power and thrust coefficients tend to become relatively independent of the freestream velocity. However, at higher freestream velocities and Reynolds numbers, the flow around the turbine blades becomes more turbulent and fully turbulent. In this regime, the flow tends to become more independent of the freestream velocity, and the power and thrust coefficients reach a relatively stable value (fully turbulent

regime). In the fully turbulent regime, the aerodynamic forces acting on the wind turbine blades, such as lift and drag, stabilize, and the power and thrust coefficients tend to reach an asymptotic value.

1.8 Uncertainty analysis

Uncertainty analysis is a vital part of any experimental program or measurement system design. It involves evaluating and quantifying the uncertainties associated with the measurements and results obtained during the experimental process. By conducting an uncertainty analysis, researchers can assess the reliability and accuracy of their measurements, identify potential sources of error, and determine the overall confidence in the obtained results. This analysis helps ensure that the experimental data is robust, reliable, and can be appropriately interpreted and compared with other studies or theoretical models. Ultimately, incorporating uncertainty analysis enhances the quality and validity of experimental research in various fields. In the early phases of experiment design, it is often impractical to distinguish between systematic and random uncertainties. Systematic uncertainties arise from biases or inaccuracies in the measurement process, while random uncertainties result from inherent variability and noise in the measurements. As the experiment progresses and more data is collected, it becomes possible to analyze the sources of uncertainty and differentiate between both effects. This analysis can provide valuable insights for refining the experimental setup, improving measurement techniques, and reducing overall uncertainty in subsequent experiments.

Uncertainty estimates should consider the imprecision in the measurements (random uncertainty) and an estimated maximum fixed error (systematic uncertainty) (Anthony J. Wheeler, Ahmad R. Ganji, 2010). In order to ensure consistency and comparability, it is important to make all uncertainty estimates to the same confidence level. The confidence level represents the degree of certainty or probability associated with the uncertainty estimate. Typically, a common confidence level of 95% is used in scientific research, which implies that there is a 95% probability that the true value lies within the estimated range. An estimate for the uncertainty is given by:

$$\omega_R = \left(\sum_{i=1}^{n} \left[\omega_{x_i} \frac{\partial R}{\partial x_i}\right]^2\right)^{1/2} \qquad \textbf{(11)}$$

Equation **(11)** is known as the "root of the sum of the squares (RSS)". When using the Root Sum Square (RSS) equation to combine uncertainties, the resulting uncertainty in the final result, R, will have the same confidence level as the individual uncertainties (x_i's) being combined. Hence, all uncertainties used in equation **(11)** must be evaluated at the same confidence level. The RSS method assumes that the uncertainties are independent and normally distributed.

The random uncertainty (P_x) is estimated using the t-distribution, determined from:

$$P_x = \pm t \frac{S_x}{\sqrt{n}} \qquad \textbf{(12)}$$

Where,

t = Students's t for 95 % of confidence level

$$\frac{\alpha}{2} = \frac{1 - 0.95}{2} = 0.025$$

Look Table 6.6 Student's t as a Function of α and ϑ (Anthony J. Wheeler, Ahmad R. Ganji, 2010).

ϑ (degree of freedom)= ∞, because of the high number of samples, then,

t= 1.96,

$\frac{S_x}{\sqrt{n}}$= the estimate of the standard deviation of the mean.

The systematic uncertainty (B_x) values often stem from limitations in equipment calibration, measurement techniques, environmental conditions, or other systematic effects, and to determine these values, a systematic error analysis should be performed, carefully considering potential sources of systematic error and evaluating their impact on the measurement process.

Finally, random and systematic uncertainties are combined to obtain the "total uncertainty", using RSS. For the mean of x:

$$\omega_x = (B_x^2 + P_x^2)^{1/2} \qquad \textbf{(13)}$$

The Rule of Propagation of Uncertainty allows to find the total uncertainty of each coefficient (C_p and C_t in the case of this study).

2 METHODOLOGY

This section consists of the description of the different parts of the project and the methodology to be followed in the laboratory.

2.1 Active grid

An active grid is needed to generate a variety of different turbulent wind fields in a large wind tunnel. The largest grid that exists actually is an aluminum frame construction of 3 m x 3 m (Universität Oldenburg, 2022), used in a large Oldenburg wind tunnel. It has almost 1,000 rhombic aluminum wings mounted on 80 individually controllable shafts. The active grid used in this study is shown in the next image, Figure 21. It has the same cross-section as the wind tunnel, 1.80 m (height) x 2.71 m (width) and it is made of orthogonal rods with vanes attached to them. In total, the active grid consists of 90 rods with vanes (shafts), where each shaft is controlled by a dedicated integrated stepper motor (Applied Motion Products Model No. STM23S-3RE) with integrated drive and encoder. Each vertical rod includes 18 diamond vanes with a diagonal of 95 mm (69 mm x 69 mm) and the horizontal rods include 27 similar vanes (Tarald Wærness, 2021). The vanes are evenly spaced, resulting in a mesh length of M = 100 mm. A horizontal bar placed at mid-height gives a 9.7 mm blockage, similar to that of the rods. In addition, in the center of the structure there are three vertical bars of 12.7 mm thickness, and 700 mm on each side of the center.

In order to achieve homogeneous and isotropic turbulence, the shafts were operated in completely random modes, with acceleration, rotational periods and rotational frequency. The shafts were controlled individually using a MATLAB script, already crated by the responsible of the wind tunnel, where the implemented driving algorithm created a fully random sequence. This allowed for varying the rotation frequency, $\Omega \pm \omega$, of the rods in the active grid to produce the three turbulent test cases: 3 %, 8 % and 13 %. Due to the arbitrary nature of the rotations, ω is a random frequency up to 1/2 Ω.

Figure 21. Active grid used for the tests.

2.2 Wind tunnel

The large-scale enclosed wind tunnel at the Fluid Mechanics Laboratory of the Norwegian University of Science and Technology (NTNU) is where the experiments were conducted. The measurements of the wind tunnel are: 1.80 m (height) x 2.71 m (width) x 11 m (length). Although the laboratory's wind tunnel has been used for numerous studies, the last one closely related to this project, Tarald's (Tarald Wærness, 2021), it has just been refurbished. The wind tunnel operates between 0 and 25 m/s in theory. For this study, stablished wind speed constant was U = 9.8 m/s for all test cases, although more speeds had to be taken for different reasons. The choice of different constant wind speeds:

- Reference wind speed: 9.8 m/s and 16 m/s. It was chosen as a trade-off between increasing the Reynolds number in the wind tunnel tests and the physical and safety limitations of the wind tunnel walls, the active grid operating range, and the wind turbine model.
- Low turbulence wind speed (3 %): 9.8 m/s and 12.5 m/s. With U= 9.8 m/s Reynold's effect appeared and the results were not acceptable.
- Medium turbulence wind speed (8 %): 9.8 m/s.
- High turbulence wind speed (13 %): 9.8 m/s.

Figure 22. Wind tunnel, Fluid Mechanics Laboratory.

2.3 Wind turbine models

In this work three types of wind turbine models were studied: straight blades and swept blades (forward and backward). The reference model was with straight blades.

The wind turbine blades used were manufactured for the previous study (Tarald Wærness, 2021), but their manufacture will be described below. These blades were adopted from a baseline wind turbine model with straight blades that had previously been tested in the wind tunnel at NTNU (Krogstad P.Å., Lund J.A., 2011) (Krogstad PÅ, Adaramola MS., 2011) (M.S. Adaramola, P.-Å. Krogstad, 2011). All three models were made from the same material to eliminate possible influences from material properties. The chosen was Ebaboard PW920, because of its relatively high stiffness and edge stability, and its lower cost compared to other stiffer materials. In order to cut the blades of the wind turbines from a single solid piece of material, a CNC machine installed in the Fluid Mechanics Laboratory was used, and after that, they need to remove additional support structures being sanded with differing grades of sandpaper. The finest grade was P1000, resulting in a smooth finish throughout the blade span. To develop the geometry of the blades a Blade Element Momentum method was used with Prandtl's tip loss model and Glauert's correction for the thrust force incorporated (Krogstad P.Å., Lund J.A., 2011). The design tip speed ratio used was $\lambda = 6$.

2.3.1 Airfoils

Following the previous study, the blade base model consists of straight blades with the NREL S826 airfoil (Figure 23) (Krogstad PÅ, Adaramola MS., 2011) across the entire blade span, concretely designed for wind turbines and with good results in wind tunnels.

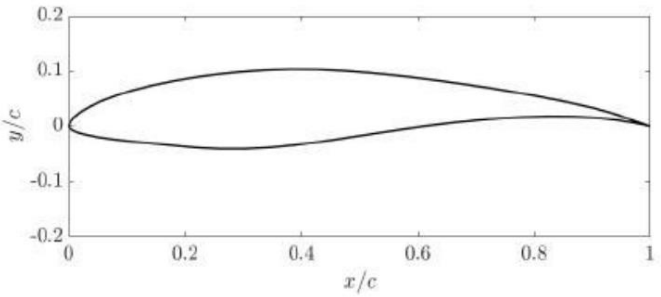

Figure 23. NREL S826 airfoil, implemented in the wind turbine models.

As a particularity, a separation ramp was designed at the back to give high maximum lift, gentle stall, and insensitivity to surface roughness. A study (Leon Li, R. Jason Hearst, 2021) found that an increase in T_i increases also the maximum lift for this particular airfoil, in particular at higher intensities of turbulence.

Figure 24 shows the characteristics of the blade: φ, the blade twist angle; c/R, normalized airfoil chord length; and both values for each blade element with normalized local radius, r/R.

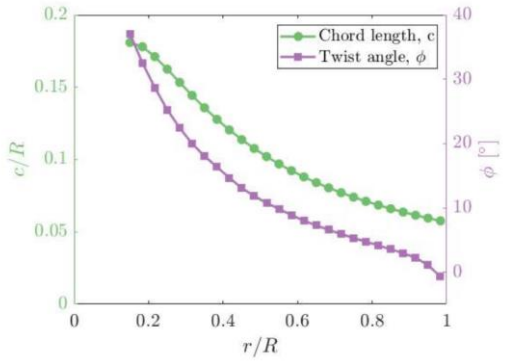

Figure 24. Chord length and twist angle distribution for each blade element. The values were used for all the wind turbine models in this study. (Source: Tarald's Master's Thesis).

In practice, to facilitate easier attachment to the hub, a cylinder with a diameter d=0.025 m was used in place of the NREL S826 airfoil towards the root of the blade (where r/R < 0.1), as shown in Figure 25. In this wind turbine model, the chord length is approximately three times wider than what is typically observed in commercial wind turbines. The main reason for using relatively wider blades was to minimize the discrepancy in Reynolds numbers. This is particularly advantageous in wind tunnel experiments where the Reynolds number (Re) tends to be significantly lower than that of utility-scale wind turbines.

2.3.2 Blades

The blades used for this study were manufactured for the previous study, so that, the the following description is based on it.

To design the curve of a swept blade, Kaya (Mehmet Numan Kaya, 2018) created an equation (14):

$$Z_s = \frac{(r_r - r_{ss})P_{ds}R/(R - r_{ss})}{M_s^{((1-P_r)(1-P_{rss})/P_r)}}$$

(14)

Where,

Z_s= sweep offset in the rotational plane,

r_r = the projected radial distance of each element onto the pitch axis,

r_{ss}= the sweep startup,

M_s= a constant that dictates the strength of the sweep.

This equation (14) is used to simply specify the design parameters for the start of the blade sweep $P_{rss} = r_{ss}/R$, and the tip displacement, $P_{ds} = d_s/R$, relative to the radius of the blade.

Table 1. Overview of utilized wind turbine models (Tarald Wærness, 2021).

Blade Sweep	*R [m]*	*P_{rss}= r_{ss}/R*	*P_{ds}= d_s/R*	*Material*
Forward swept	0.45	0.35	0.20	Ebaboard PW920
Backward swept	0.45	0.35	0.20	Ebaboard PW920
Straight	0.45	0.00	0.00	Ebaboard PW920

In the preliminary study, the Blade Element Momentum (BEM) method, a well-established approach, was employed. The blade span was divided into 30 elements, as shown in Figure 24. The software ASHES (Simis, 2023) was utilized, which incorporates a standard implementation of the BEM method. Notably, the software has recently been updated to include the capability of analyzing swept blades, enhancing its functionality and versatility. According to the results obtained from ASHES, the highest degree of blade sweep exhibited the most significant effects. These findings highlight the importance and impact of blade sweep on the observed outcomes (maximum value of tip offset, P_{ds} = 0.20). Although this agrees with Kaya's studies, the results for the blade sweep startup exhibited variations. Taking into account the variations observed and the physical constraints of the manufacturing process, the following design parameters were chosen for both the forward and backward swept blades: P_{ds} = 0.20 and P_{rss} = 0.35. These parameters were determined to be suitable for achieving the desired outcomes while considering the limitations imposed by the manufacturing process, summary Table 1.

In addition, an independent model with straight blades was created to isolate the effect of blade sweep on the wind turbine blades. Thus, nine wind turbine blades were manufactured Figure 25.

Figure 25. The back view of the three wind turbine blades used in the study, created in the study before (Tarald's Master's Thesis), forward swept (left), straight (middle), backward swept (right). Each set of three blades were mounted to the experimental setup with two metal clamps.

To minimize the influence of the rotor-swept area, a constant radius was maintained for all the blades. By keeping the radius consistent, any variations observed in the results can be attributed mainly to the differences in blade design parameters and not the changes in the rotor-swept area, $A = \pi R^2$. This approach allows for a more focused analysis of the impact of blade sweep and other design factors on the overall performance of the wind turbine, independent of the rotor size. The swept blades exhibit a slight increase in rotor solidity, which is defined as the total blade area divided by the rotor-swept area. This increase in solidity is due to the curved length of the swept blades covering a slightly larger portion of the rotor-swept area compared to the straight blades. The curvature of the swept blades results in a higher blade area within the rotor-swept region, contributing to the elevated rotor solidity value. Since the forward and backward swept blades were identical except for the sweep direction, their solidity would indeed be equal.

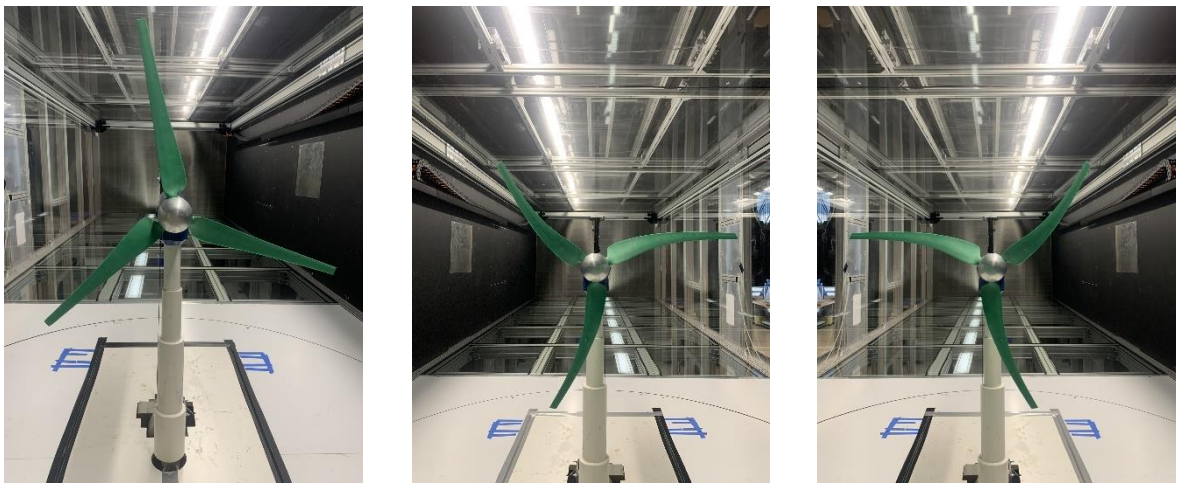

(a) (b) (c)

Figure 26. Attached to the experimental setup are wind turbine models, viewed from the front. Each model consists of an aluminum hub connected to different types of blades: (a) straight blades, (b) forward-swept blades and (c) backward-swept blades. It's important to note that all models rotate in a clockwise direction.

2.4 Experimental setup

The entire installation was assembled following Tarald's work, as shown in the following scheme, Figure 27. From right to left, the wind turbine system consists of a tower shaft, a nacelle, and a rotor shaft located within the nacelle. The rotor shaft directly connects to a belt-drive electric motor. The tower shaft provides structural support for the turbine, while the nacelle houses essential components such as the rotor shaft and the electric motor. The rotor shaft, which is connected to the blades, transfers the rotational motion to the belt-drive electric motor, converting the wind energy into electrical energy. Inside this horizontal shaft there is a torque transducer to measure the torque and an optical sensor, to measure the rpm.

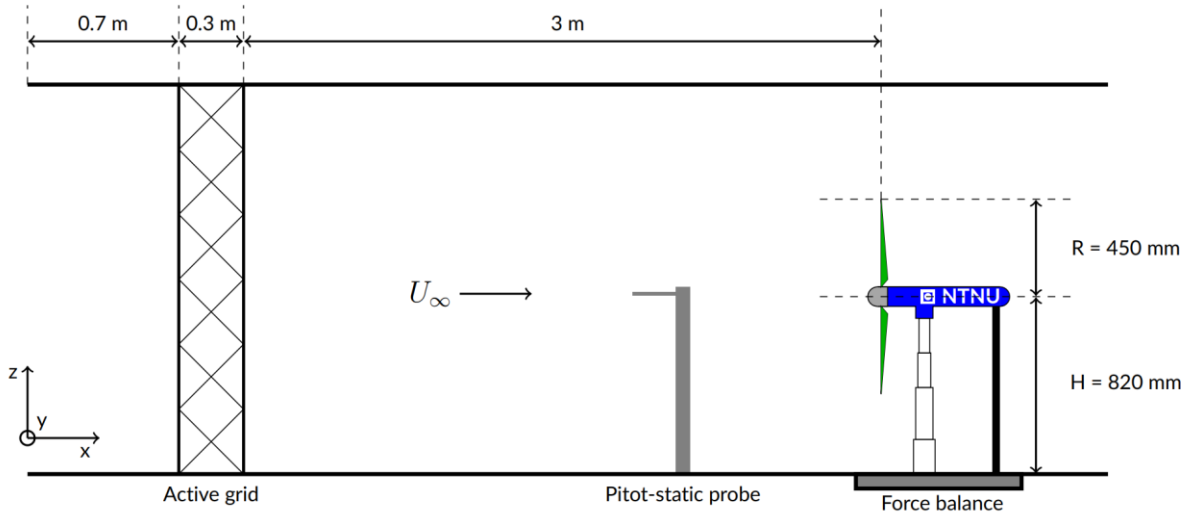

Figure 27. Schematic of the side view of the experimental setup in the wind tunnel. (Source: Tarald's Master's Thesis).

At one end of the rotor shaft, there is a metal plate designed to allow direct mounting of the wind turbine models. This metal plate serves as a secure attachment point for the wind turbine models, enabling them to be directly mounted onto the rotor shaft. This arrangement ensures stability and proper alignment of the models during testing and operation. A 90mm diameter aluminum hub is used to fit the current setup, and all three models of wind turbines were directly connected. The hub height, denoted as H, was set at 820 mm above the wind tunnel floor. This measurement refers to the vertical distance from the base of the wind tunnel to the hub of the wind turbine models.

All the wind turbine is mounted in a force balance, to measure the forces before starting the tests.

The distance from the active grid to the hub's location was 3 m. The active grid, used for controlling and manipulating the airflow, was positioned at a distance of 0.7 m from the wind tunnel inlet. The support structure of the grid had a width of 0.3 m. This configuration allowed for precise control and manipulation of the airflow entering the wind tunnel, facilitating accurate testing and analysis of the

wind turbine models. This distance is a relative distance along the current of x/M= 30, where M = 100 mm is the mesh length of the grid. A pitot-static probe was installed between the wind turbine and the grid to measure.

If the shaft was mounted at a height of 820 mm, the lowest elevation of the blades during rotation was 370 mm. Previous studies have measured the location of the wind turbine hub to be outside of the ground plane boundary layer within the wind tunnel. This positioning ensures that the hub is situated in a region of the wind tunnel where the airflow remains unaffected by the ground boundary layer.

To control and monitor the rotor speed of the wind turbine models, a SIEMENS MICROMASTER 440 frequency converter was utilized. This frequency converter (Figure 28) was connected to a 0.43 kW SIEMENS AC electric motor. The electric motor, with a maximum rotational speed of approximately 3000 rpm, facilitated the adjustment and monitoring of the rotor speed. The frequency converter provided precise control over the motor's frequency, enabling accurate regulation of the wind turbine's rotational speed during the experiments, varying the rotational speed of the wind turbine models between $20 \leq \omega \leq 300$ [rad/s]. This corresponds to the tip speed ratio range between $1 \leq \lambda \leq 10$. The frequency converter was connected to a resistor (Figure 29) to be able to give the needed frequencies.

Figure 28. Frequency converter used in the study.

Figure 29. Resistor used in this study.

In this study, the model blockage ratio was determined to be 13% (Tarald Wærness, 2021). The model blockage ratio is calculated by dividing the rotor-swept area (A) by the wind tunnel's cross-sectional area (At). A blockage ratio of 13% indicates that the wind turbine models occupied approximately 13% of the total cross-sectional area of the wind tunnel. This ratio is important for evaluating the influence of the wind turbine models on the airflow within the wind tunnel and understanding the potential flow disruptions caused by the presence of the models.

2.5 Measurement equipment and uncertainties

To measure the aerodynamic power of the wind turbine models, a torque transducer was employed. The power (P) was calculated using the equation $P = Q\omega$, where Q represents the net torque measured by the torque transducer, and ω corresponds to the angular velocity of the wind turbine rotor. By measuring the torque exerted by the wind on the turbine blades and combining it with the rotor's angular velocity, the aerodynamic power generated by the wind turbine models could be accurately determined using this equation. The output data were acquired using in-house LabVIEW software, at a sampling speed of 50.000 kS/s, 5,000 S/ch and for a total of 2 minutes for reference and low turbulence casevfor each sample, being this duration sufficient to provide data to analyze the performance under these conditions. For the medium and high turbulence intensities, the data collection period was extended to 6 minutes for each sample. This longer duration was necessary to capture and analyze the effects of increased turbulence on the aerodynamic performance. The freestream reference velocity in this study was determined by measuring the pressure using a Pitot-static pressure probe. The temperature and atmospheric pressure in the wind tunnel were measured using specific instruments. Temperature was measured directly by the LabVIEW program and a thermometer, while a precision mercury barometer was employed to measure the atmospheric pressure every day.

To obtain the total measurement uncertainties for each measurement point, a combination of random and systematic uncertainties was considered, as explained at (Anthony J. Wheeler, Ahmad R. Ganji, 2010). The random uncertainties were

computed for a 95% confidence interval from the measured signals. The systematic uncertainties in the measurement equipment were found to be the major contributors to the overall uncertainties (values obtained from the supervisor). Systematic uncertainties arise from factors that cause consistent biases or errors in the measurements. These can be due to limitations or imperfections in the measurement instruments, calibration procedures, environmental conditions, or other systematic effects that impact the measurement process.

Table 2. Values to calculate the systematic uncertainty.

Parameter	*Accuracy*
RPM	+- 1RPM
Torque transducer	+- 1.00E-8
Load cells	+- 0.02 V
Barometer (inaccuracy on reading)	+- 0.2 mmHg
Thermocouple	+- 0.5 deg
Pressure transducer	+- 0.1% of the reading

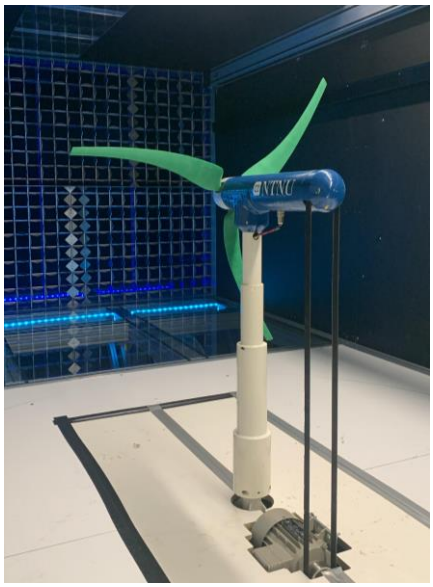

Figure 30. Wind turbine model with forward sweep blades and the active grid.

3 RESULTS AND DISCUSSION

The aerodynamic performance of a wind turbine model is determined by how its power output and thrust behave at different wind speeds. When the wind speed remains constant, we can calculate the power coefficient C_P (1) and thrust coefficient C_T (3) by adjusting the rotor's rotational velocity over a wide range of tip speed ratios λ (2). In this section, there are presented the average values and corresponding uncertainties of the power and thrust coefficients for the wind turbine models described in Table 1. To enhance readability, the error bars only highlight the tip speed ratio range that is most significant, but it is assumed that the errors remained relatively constant for all the measurements. For this assumption, due to the nature of post processing, which requires time and lack of time, the error has been calculated only for one TSR (C_{Pmax}) per each blade setup. In this study, the dependence on Reynolds number is an important aspect that is being discussed.

First of all, mention that the negative points plotted in the Cp graphs are not valid, since the objective is to give power, not to consume.

It is also important to emphasize again, since this thesis is the continuation of Tarald's thesis (Tarald Wærness, 2021), that the tests have been repeated increasing the sampling time: 2 or 6 minutes, depending on the case of turbulence.

3.1 Reynolds number effect

From the previous study, it was concluded that the resulting airfoil profiles were affected by the relatively high tolerance (Tarald Wærness, 2021). The tip of the wind turbine blades, particularly the trailing edge, experiences notable effects due to its unique design, where the trailing edge is cut off compared to the standard NREL S826 airfoil profile. In truth, reducing the airfoil chord length, denoted as c, directly decreases the experienced Re. Reinolds number is directly proportional to the characteristic length of the flow (in this case, the airfoil chord length) and the freestream velocity.

However, although the study focused on a wind speed U= 9.8 m/s, at that velocity the power and thrust coefficients were still Re dependent for the no turbulence (reference Ti= 1 %) and low turbulence (Ti= 3 %) setups, see Appendix Additional Results 4.1.1 and 4.1.2. Consequently, the freestream velocity for reference experiment was increased to U= 16 m/s and for the low turbulence experiment U= 12.5 m/s. Despite the limitations in the range of operation of the active grid and the safety concerns with the models of wind turbines due to high speeds, increasing the sampling time, acceptable results have been obtained.

3.2 Reference

As mentioned previosuly, the results from the reference test case showed Re-dependent behavior ($U\infty$ < 12.5 m/s). The data collection of the experiment without active grid, Ti=1 %, and wind speed of U= 16 m/s and 2 minutes of sampling time, gave the following results, for the three configurations of blades.

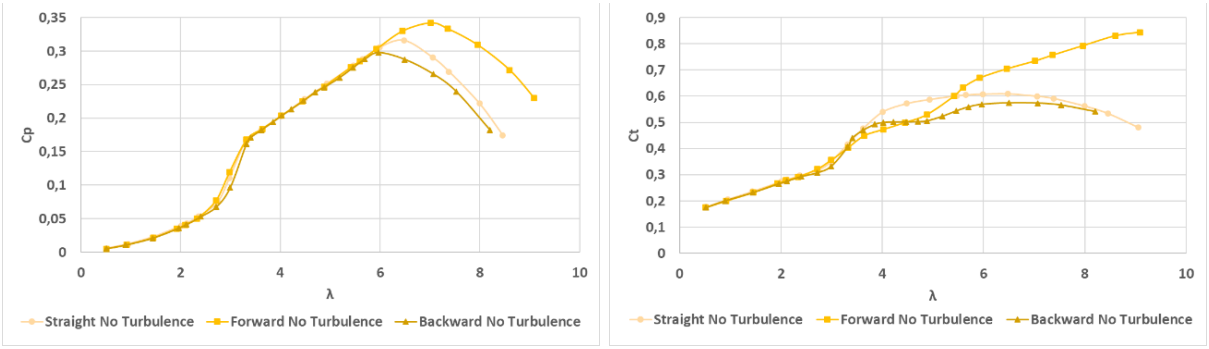

(a) (b)

Figure 31. Effects of blade sweep for the wind turbine models with straight blades, forward swept and backward swept. (a) power coefficients C_p and (b) thrust coefficients C_T at different tip speed ratios, λ. The figure depicts the reference test case, without active grid (Ti = 1 %). The reference velocity was kept constant at U = 16 m/s for all the test cases. Thus, the tip speed ratio was only varying with the rotational velocity of the rotors, ω.

The obtained results for power coefficients are very similar for the three blades tests until λ ≈ 6, after that point forward sweep blades C_p values got an improvement, but, at the same time C_T values also started to increase linearly. Straight blades and backward sweep blades have close behaviour, although the results of straight blades are better, higher power coefficient.

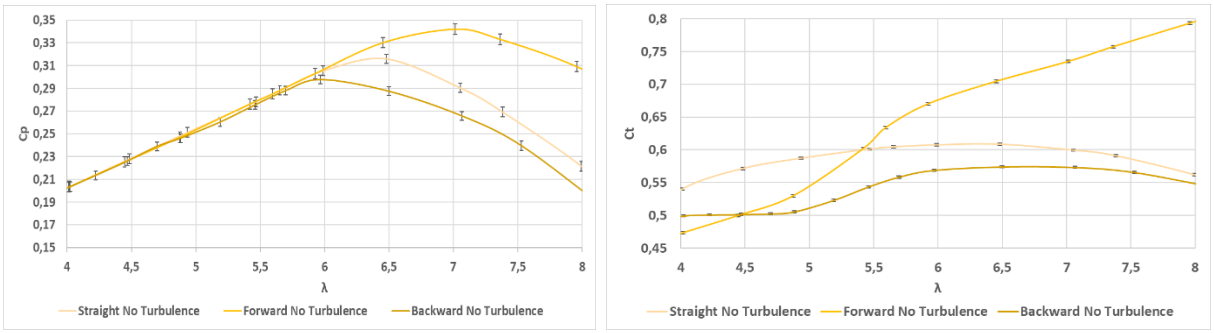

(c) (d)

Figure 32. Uncertainty analysis for reference test case, without active grid (Ti= 1 %) and U= 16 m/s. Error bars for C_P (c) and C_T (d) are shown in a zoomed view for the most interesting parts of the data.

As mentioned before in chapter 3, both uncertainties, for power coefficient and for thrust coefficient, were calculated assuming the error ocurred in the maximum C_P value of each blade test. The uncertainty analysis for C_P (c) demostrated that until

λ ≈ 6, error bars overlap, so no distinction is made in the three types of blades (agrees with the results Figure 31). But, after λ ≈ 6, the curves disperse and the error bars are not overlaped, so the different types of blades have an influence on the power. On the other side, in the analysis for C_T (d), the bars never overlap, and it is concluded that the 3 types of blades have an influence on the coefficient.

Table 3. Max power coefficients, C_{pmax}, with the corresponding tip speed ratios, λ, and thrust coefficients, C_T, for reference test case.

					Power coefficient			*Thrust coefficient*		
Test case	*Blade Sweep*	*Ti [%]*	*U [m/s]*	*λ*	*Cp max*	*Uncertainty*	*ΔCPmax*	*Ct*	*Uncertainty*	*ΔCT*
Ref Straight	*S*	1	16	6,48	0,32	0,42%		0,61	0,18%	
Ref Forward	*F*	1	16	7,01	0,34	0,46%	8,26%	0,73	0,21%	20,75%
Ref Backward	*B*	1	16	5,97	0,30	0,39%	-5,78%	0,57	0,17%	-6,56%

Where,

$$\Delta C_{P_{max,F}} = \frac{C_{P_{max,F}} - C_{P_{max,S}}}{C_{P_{max,S}}};\ \Delta C_{P_{max,B}} = \frac{C_{P_{max,B}} - C_{P_{max,S}}}{C_{P_{max,S}}}$$

$$\Delta C_{T_F} = \frac{C_{T_F} - C_{T_S}}{C_{T_S}};\ \Delta C_{T_B} = \frac{C_{T_B} - C_{T_S}}{C_{T_S}}$$

3.3 Effects of the blade sweep

The primary focus of this study was to analyze and compare the aerodynamic performance of a wind turbine model equipped with forward swept blades and backward swept blades. The objective was to investigate and understand the effects of blade sweep on the turbine's overall power and thrust.

In this chapter, the effect generated by the different types of blades will be compared, in the three turbulence samples (Ti= 3 %, Ti= 8 % and Ti= 13 %).

3.3.1 Low turbulence (Ti= 3 %)

For this test case, the installed active grid was in static mode and the sampling time was 2 minutes. The results (Figure 33) indicate that the wind turbine model with straight blades outperformed the models with swept blades after λ ≈ 4.3, regardless of the sweep direction (forward or backward). This finding suggests that the straight blade configuration exhibited superior aerodynamic performance in terms of efficiency, power output, or other relevant performance metrics compared to the swept blade configurations. The reasons for the superior performance of the straight blades could be attributed to several factors: simpler and more uniform design and geometry, which can result in smoother airflow and reduced aerodynamic losses; less flow separation and turbulence compared to swept

blades, leading to higher lift-to-drag ratios and improved efficiency. It is important to note that these findings are specific to the wind turbine models and conditions investigated in the study. The performance of wind turbine blades can vary depending on various factors, including the specific design parameters, wind conditions, and operational considerations.

In high tip speed ratios, λ > 6.8, forward swept blades have the highest power output. Forward swept blades may exhibit improved flow behavior and better utilization of the incoming wind energy under these conditions, resulting in increased power extraction due to their specific aerodynamic characteristics. And though there are some shaky points, the power coefficients for all the models follow a wind turbine's expected power curve characteristics (Figure 33).

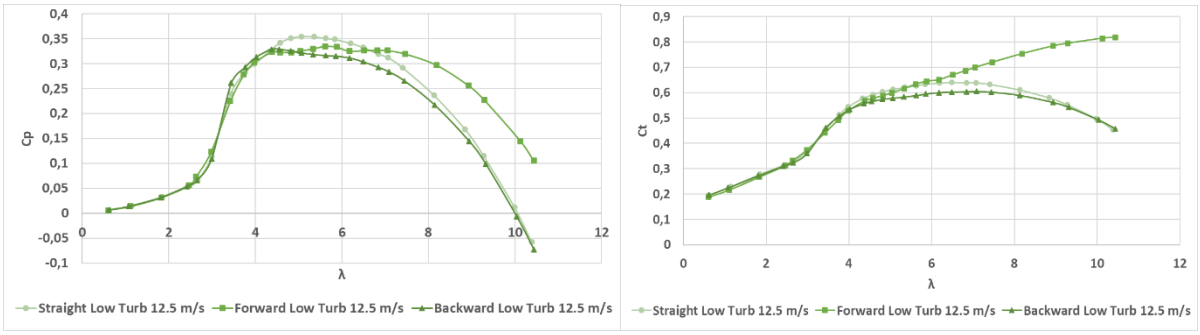

(a) (b)

Figure 33. Effects of blade sweep for the wind turbine models with straight blades, forward swept and backward swept. (a) power coefficients Cp and (b) thrust coefficients CT at different tip speed ratios, λ. The figure depicts the low turbulence test case (Ti = 3 %). The reference velocity was kept constant at U = 12.5 m/s for all the test cases. Thus, the tip speed ratio was only varying with the rotational velocity of the rotors, ω.

Simultaneously, C_T values for 3 blades are close to each other until λ ≈ 3.8, where they start separating being the straight blades worth over until λ ≈ 5.3. In this point, forward blades C_T starts increasing quite linearly, and the other two have the same downward trend. The linear increase in C_T for forward blades indicates a positive correlation between the blade sweep and thrust efficiency. This suggests that the forward blade configuration effectively harnesses the incoming wind flow, resulting in an enhanced thrust coefficient. The linear relationship suggests that as the wind speed or rotational speed of the turbine increases, the C_T value will continue to rise proportionally (see 1.5.2), a high thrust coefficient can be desirable because it indicates that the wind turbine is effectively converting a larger portion of the incoming wind's kinetic energy into thrust force. It is evident that backward swept blades experience a more significant decrease in the thrust coefficient compared to forward swept blades, while achieving approximately the same maximum power output.

The maximum values for the power coefficients, C_{Pmax}, were 5.46 % and 7.21 % lower (Table 4) for the forward and backward swept blades, respectively, compared to the straight blades. And 3.21 % higher for forward and 8.01 % lower for backward blades compared to straight ones in the case of C_T.

Relating this to the analysis of uncertainties, as mentioned earlier in chapter 3, the uncertainties for both the power coefficient (C_P) and thrust coefficient (C_T) were calculated assuming that the error occurred in the maximum C_P value of each blade test. This means that the maximum C_P value obtained for each blade configuration was used as the basis for estimating the uncertainties associated with C_P and C_T.

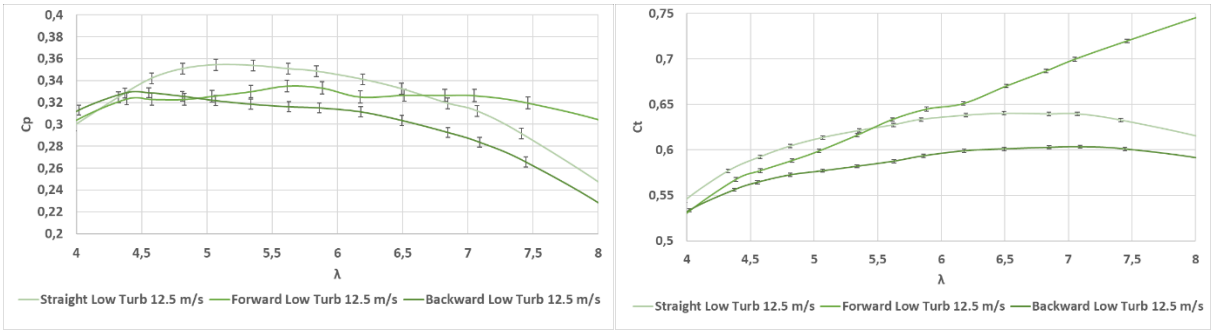

(c) (d)

Figure 34. Uncertainty analysis for low turbulence test case (Ti= 3 %) and U= 12.5 m/s. Error bars for C_P (c) and C_T (d) are shown in a zoomed view for the most interesting parts of the data.

The zoomed area of the Figure 34 (c) demostrates that in the most critic area (from $\lambda \approx 4$ to $\lambda \approx 8$) there are overlaped error strips, this means that it cannot be said that the three cases are different, since this superposition demonstrates that due to random or systematic uncertainties, these values could undergo changes, until the points of two curves change position (larger or more little). Nonetheless, since $\lambda \approx 4.5$ to $\lambda \approx 6.5$ clearly straight blades have higher power, and in $\lambda > 7$ forward blades outperform the other two, and the backward ones give the worse value. For graph (d) Figure 34, it can clearly be said that the influence of the geometry of the blades is noticeable, except between $5.3 \approx \lambda \approx 5.8$.

Table 4. Max power coefficients, C_{pmax}, with the corresponding tip speed ratios, λ, and thrust coefficients, C_T, for low turbulence test case.

Test case	*Blade Sweep*	*Ti [%]*	*U [m/s]*	*λ*	*Cp max*	*Uncertainty*	*ΔCpmax*	*Ct*	*Uncertainty*	*ΔCt*
Low Turb Straight	*S*	3	12.5	5,07	0,35	0,50%		0,61	0,19%	
Low Turb Forward	*F*	3	12.5	5,61	0,34	0,55%	-5,46%	0,63	0,20%	3,21%
Low Turb Backward	*B*	3	12.5	4,55	0,33	0,45%	-7,21%	0,56	0,18%	-8,01%

3.3.2 Medium turbulence (Ti= 8 %)

For the medium turbulence test case, the installed active grid was configurated with intensity around 8 % and the sampling time was 6 minutes. The behavior is very similar to the case of low turbulence. The results for power (Figure 35, (a)) indicate that the wind turbine model with straight blades outperformed the models with swept blades after $\lambda \approx 3.5$ until $\lambda \approx 8.3$. In that point, forward blades take advantage. On the other hand, observing the graph for C_T (b) at $\lambda \approx 7.2$ the coefficient lines of straigh and forward intersect, linearly increasing the thrust

coefficient of forward ones. The power coefficients for all the models in the study exhibit characteristics that align with the expected power curve of a wind turbine.

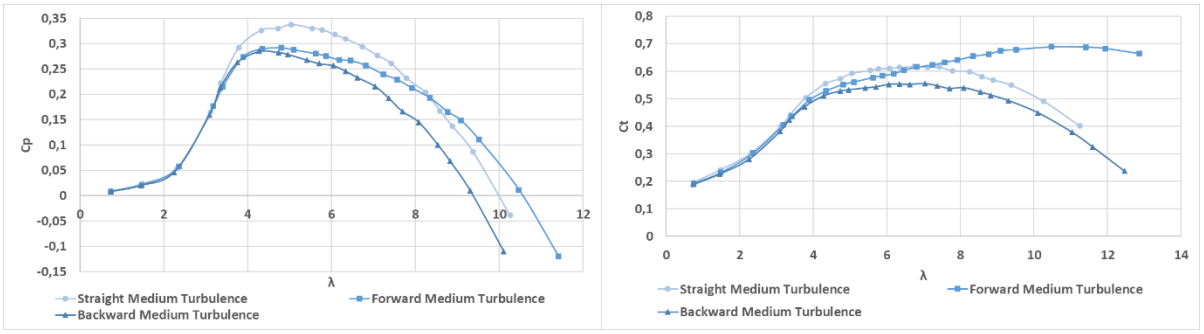

(a) (b)

Figure 35. Effects of blade sweep for the wind turbine models with straight blades, forward swept and backward swept. (a) power coefficients C_p and (b) thrust coefficients C_T at different tip speed ratios, λ. The figure depicts the medium turbulence test case (Ti = 8 %). The reference velocity was kept constant at U = 9.8 m/s for all the test cases. Thus, the tip speed ratio was only varying with the rotational velocity of the rotors, ω.

The maximum values for the power coefficients, C_{Pmax}, were 13.56 % and 15.68 % lower (Table 5) for the forward and backward swept blades, respectively, compared to the straight blades. And for thrust, 6.71 % and 13.74 % for the forward and backward swept blades, respectively, compared to straight ones.

In this point, the analysis of uncertainties follows chapter 3, as both the power coefficient (C_P) and thrust coefficient (C_T) were calculated assuming that the error happened in the C_{Pmax} of each blade test, meaning that the maximum C_{Pmax} value from each blade configuration was used as the basis for estimating the uncertainties associated with C_P and C_T.

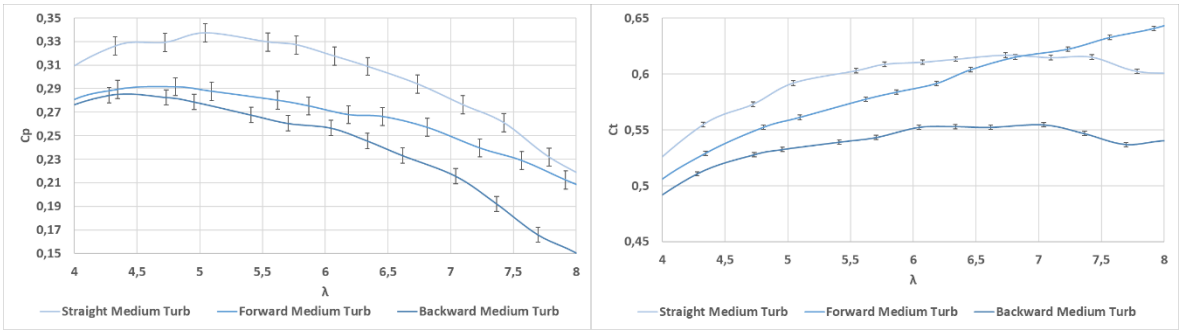

(c) (d)

Figure 36. Uncertainty analysis for medium turbulence test case (Ti= 8 %) and U= 9.8 m/s. Error bars for C_P (c) and C_T (d) are shown in a zoomed view for the most interesting parts of the data.

In the zoomed area of the Figure 36 (c) it is proved that in the most critic area (from λ ≈ 4 to λ ≈ 8) the error bars of forward blades and backward blades are overlaped until λ ≈ 4, and also straight and forward blades C_P curves suffer a coincidence after λ ≈ 7.5; this means that it is not possible to said that this two cases are different, since this superposition demonstrates that due to random or systematic uncertainties, these values could be different as plotted. For graph (d)

Figure 36, it can be said that the influence of the geometry of the blades is noticeable, except between 6.5 ≈ λ ≈ 7, that there exists an intersection between straigh and forward blades curves error bars.

Table 5. Max power coefficients, Cpmax, with the corresponding tip speed ratios, λ, and thrust coefficients, CT, for medium turbulence test case.

				Power coefficient				Thrust coefficient			
case	Blade Sweep	Ti [%]	U [m/s]	λ	Cp max	Uncertainty	ΔCpmax	Ct	Uncertainty	ΔCt
Medium Turb Straight	S	8	9.8	5,04	0,34	0,77%		0,59	0,21%	
Medium Turb Forward	F	8	9.8	4,81	0,29	0,76%	-13,56%	0,55	0,20%	-6,71%
Medium Turb Backward	B	8	9.8	4,28	0,28	0,65%	-15,68%	0,51	0,19%	-13,74%

3.3.3 High turbulence (Ti= 13 %)

In the last case, high turbulence, the turbulence intensitiy was close to 13 % and the sampling time was six minutes. Like in the two previous cases, the power coefficients for all the models in the study demonstrate characteristics that are consistent with the expected power curve of a wind turbine (Figure 37).

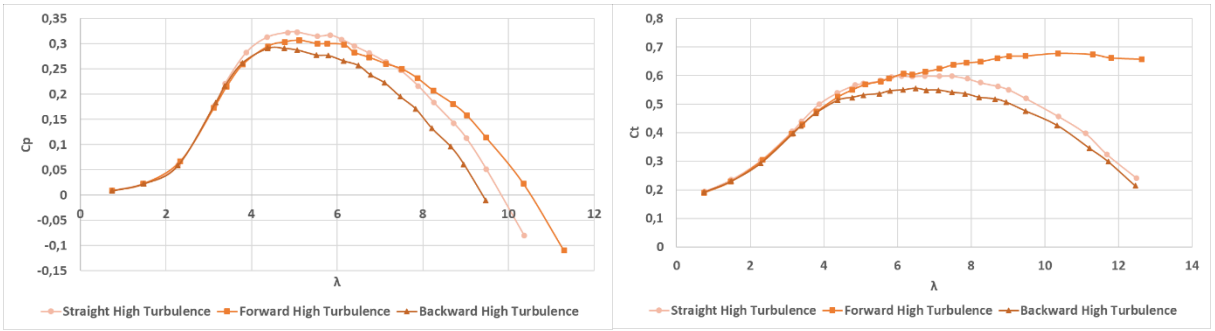

(a) (b)

Figure 37. Effects of blade sweep for the wind turbine models with straight blades, forward swept and backward swept. (a) power coefficients C_p and (b) thrust coefficients C_T at different tip speed ratios, λ. The figure depicts the high turbulence test case (Ti = 8 %). The reference velocity was kept constant at U = 9.8 m/s for all the test cases. Thus, the tip speed ratio was only varying with the rotational velocity of the rotors, ω.

Inspecting graph (a), until λ ≈ 3.4 the behaviour of the 3 blades is similar, when in the range of 3.4 < λ < 7.5 straight blades exceed swept blades models. In high TSPs again, forward blades generate more power (λ > 7.5). At the time, C_T curves (b) corroborate that btween tip speed ratio of 4.3 and 6.4 both straight balde curves and forward swept curves are almost identical, and later than this dot, one more time forward blades outstrip the rest.

Table 6 validate the maximum values for the power coefficients compared with stright blades: -4.96 % and -9.72 %, and for the thrust coefficients, -0.68 % and -10.28 %.

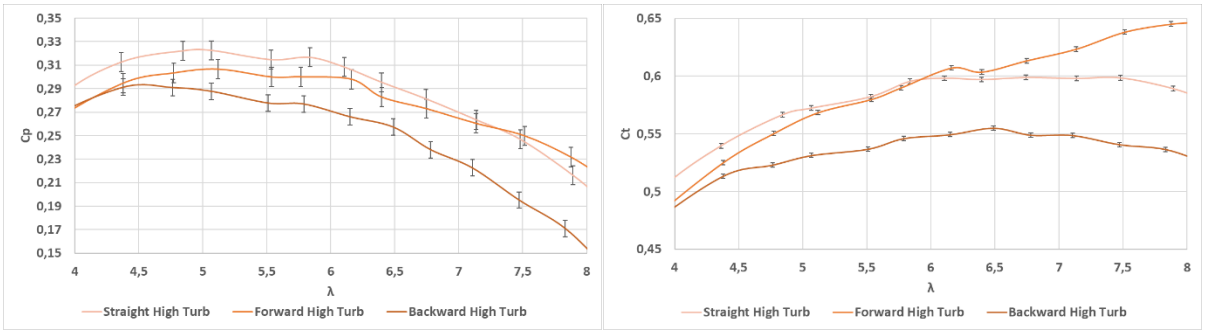

(c) (d)

Figure 38. Uncertainty analysis for high turbulence test case (Ti= 13 %) and U= 9.8 m/s. Error bars for C_P (c) and C_T (d) are shown in a zoomed view for the most interesting parts of the data.

Following the uncertainties examination in chapter 3, backward blades curve the influence given by its geometry is credible, except with small lambdas (λ < 4.5). But, straight and forward swept blades error bars match in several intervals, for C_p, both are overlaped during all the zoomed part (Figure 38 (c)), so it it is not possible to argue that the two different blade curves give different results. Same for (d) graph,results for S and F blades are not conclusive in the spectrum of TSR among 5 and 6.

Table 6. Max power coefficients, C_{pmax}, with the corresponding tip speed ratios, λ, and thrust coefficients, C_T, for high turbulence test case.

					Power coefficient			*Thrust coefficient*		
case	*Blade Sweep*	*Ti [%]*	*U [m/s]*	*λ*	*Cp max*	*Uncertainty*	*ΔCpmax*	*Ct*	*Uncertainty*	*ΔCt*
High Turb Straight	*S*	13	9.8	5,07	0,32	0,81%		0,57	0,21%	
High Turb Forward	*F*	13	9.8	5,12	0,31	0,82%	-4,96%	0,57	0,20%	-0,68%
High Turb Backward	*B*	13	9.8	4,38	0,29	0,70%	-9,72%	0,51	0,19%	-10,28%

3.4 Effects of turbulence

The effects of varying the turbulent inflow conditions are shown in the next figures (Figure 39 and Figure 40). The investigation focuses on 2 test cases, medium turbulence (T_i= 8 %) and high turbulence (T_i= 13 %), because they were the two samples where the speed was the same (U= 9.8 m/s). In general, for forward and backwad swept blades the model turbines demonstrate an increased power output as the measured turbulent characteristics increase, oposite for straight blades.

Turbulence in the wind refers to fluctuations in wind speed and direction. Turbulent flow can have a significant impact on the performance of wind turbines, so can lead to increased power generation by the wind turbine. The relationship between turbulent characteristics and power output can vary depending on the specific turbine design and operating conditions. Increased turbulence can provide a more dynamic and energetic wind flow, allowing the wind turbine to extract more energy from the wind. Turbulence can also help in reducing the adverse effects of boundary layer separation, leading to improved aerodynamic performance and increased power conversion efficiency.

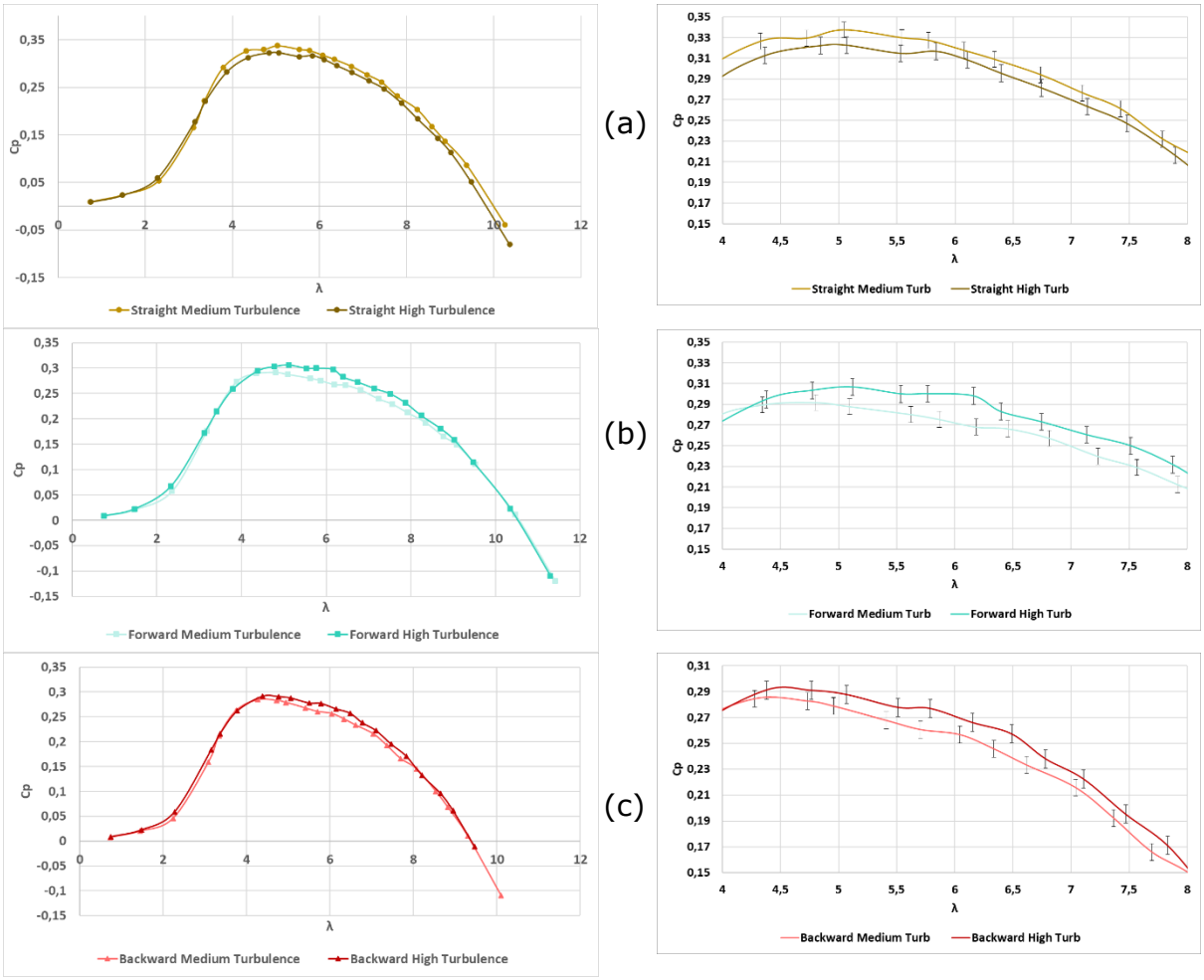

Figure 39. Effects of varying the turbulent inflow conditions on the power coefficients (C_P), of the wind turbine models at different tip speed ratios (λ). Reference velocity was constant U= 9.8 m/s for all cases and TSR only varying with the rotational velocity of the rotors (ω). Both medium intensity (8 %) and high intensity (13 %) of turbulence for straight blades (a), forward swept blades (b) and backward swept blades (c). Error bars for C_P are shown in a zoomed view for the most interesting parts of the data.

A quantifiable example of this is that the maximum power coefficient, C_{Pmax}, of the forward swept blades, increase by 7 % from test case medium turbulence case to high turbulence case, the backward swept blades increase by 3.5 %, while for the straight blades the decrease was 5.9 %. It is seen that there is no great difference between the two turbulence intensities.

As the two turbulence intensities are quite close (8% and 13%), no great difference is appreciated between the thrust coefficient curves (Figure 40).

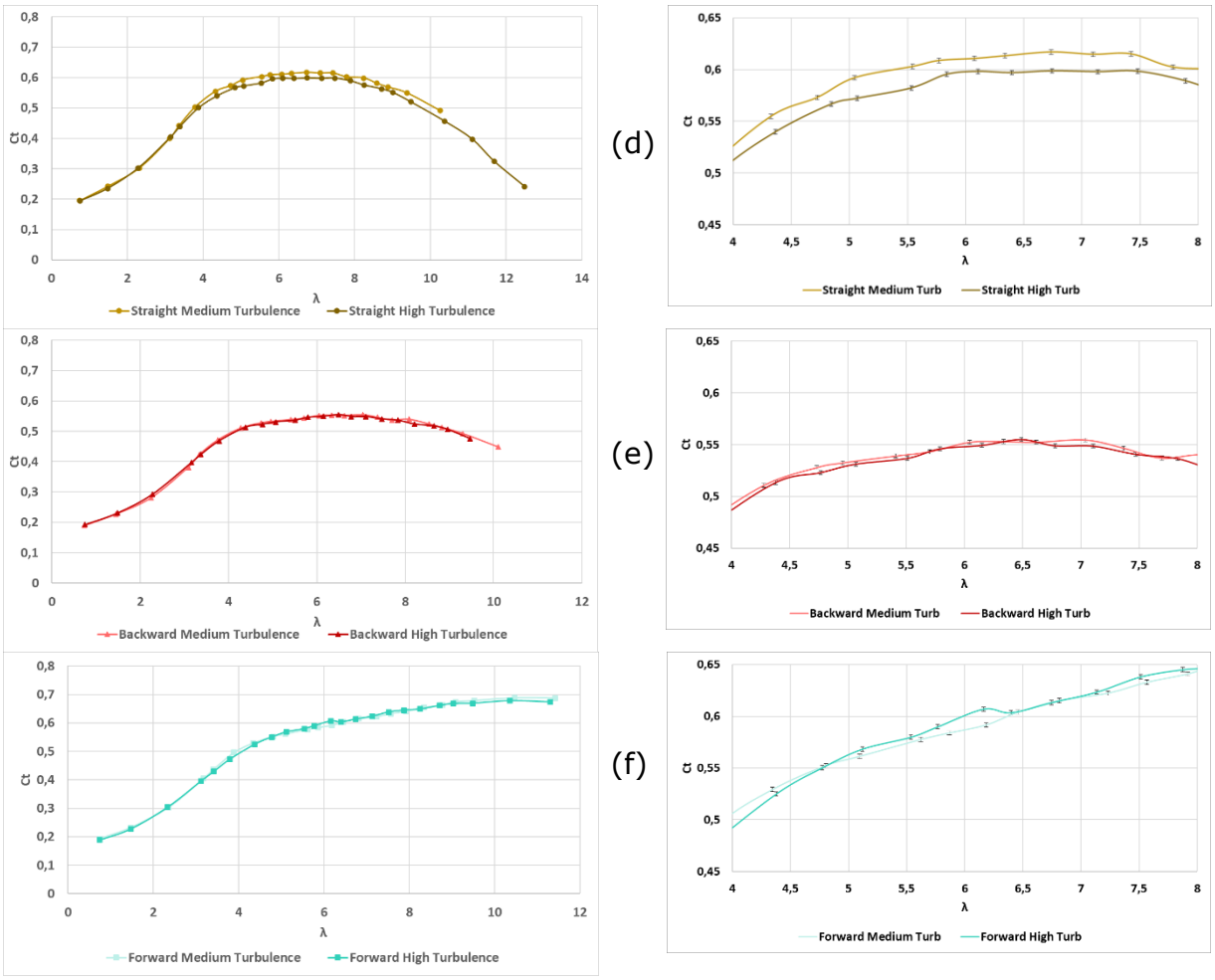

Figure 40. Effects of varying the turbulent inflow conditions on the power coefficients (C_T), of the wind turbine models at different tip speed ratios (λ). Reference velocity was constant U= 9.8 m/s for all cases and TSR only varying with the rotational velocity of the rotors (ω). Both medium intensity (8 %) and high intensity (13 %) of turbulence for straight blades (d), forward swept blades (e) and backward swept blades (f). Error bars for C_T are shown in a zoomed view for the most interesting parts of the data.

When analyzing the uncertainties, the problem arises that, except in the case of C_T and straight blades, the error bars are assumed in the others. This implies that the comparison of these two turbulence intensities does not provide much information, since it cannot be shown that the curves of both turbulences are different from each other.

4 CONCLUSIONS

This study aimed to investigate and analyze the aerodynamic performance of three horizontal axis wind turbine models featuring different blade sweep orientations. The three blade configurations examined were forward swept blades, backward swept blades, and straight blades. By conducting measurements and analyses, the study sought to gain insights into the effects of blade sweep on the aerodynamic characteristics and performance of the wind turbines. Throughout the research process, various parameters related to the aerodynamic performance of the wind turbine models were measured and analyzed. These included power output, thrust, torque, and other relevant performance indicators. The measurements were conducted under different operating conditions, such as varying wind speeds and turbulence intensities, to capture a comprehensive understanding of the performance variations among the different blade configurations. The experiments conducted in this study employed an active grid to generate controlled and consistent freestream turbulence for testing the wind turbine models, varying inflow conditions measured by the turbulence intensities, T_i. The analysis focused on three test cases in particular, low turbulence (T_i= 3 %), medium turbulence (T_i= 8 %) and high turbulence (T_i= 13 %).

Similar to the previous study, (Tarald Wærness, 2021), comparing the 2 cases with higher turbulence intencity (because both measuremets were with U= 9.8 m/s) the results obtained from reveal a notable trend: as the turbulence intensities increase, the power coefficients of the wind turbine models also show an increase. This finding suggests that higher turbulence levels have a positive impact on the power generation capabilities of the wind turbines. As the turbulence intensities established for this study have been lower than in the previous similar study, and the wind speed has also decreased, the values obtained are also lower. Despite this, as the sampling times have risen from 30 seconds to 6 minutes, the curves obtained are much more realistic and resemble the theory. However, it was observed that the different wind turbine models in the study were influenced by turbulence to varying degrees. Forward swept blades show in all the cases that it's C_P surpasses other two blade models in high TSR values. At the same time, it's C_T values also are higher, increasing linearly. In some cases, a high thrust coefficient is desirable because it indicates that the wind turbine is effectively converting a larger portion of the incoming wind's kinetic energy into thrust force. This can result in increased power generation and improved overall performance of the wind turbine. Higher thrust coefficients are often associated with greater power extraction capabilities, which can be advantageous for maximizing energy production. A higher C_T indicates a greater ability to extract energy from the wind, but it should be balanced with other considerations such as structural integrity, noise generation, and wake effects.

Thus, turbulence has been found to increase the total drag on the wind turbine system for all the models in the study, but the magnitude of this increase varies among the different models. In medium lambda values, straight blades give better results, and in small λ, the three blades have a very similar behavior. In the three experiments with turbulence, the straight blades give the best results, highest C_P values. But in the reference case, the maximum C_P is generated by the forward blades, then straight blades and finally backward blades.

As this is a new study associated with the initial project of " An experimental study of the performance of a wind turbine model with swept blades, for different inflow conditions", but with a longer sampling time, it should be noted that the curves obtained have been realistic. Meaning, the power coefficients observed for all the wind turbine models in the study exhibit characteristics that are consistent with the expected power curve of a wind turbine. Still, for further study, the experiment could be repeated with higher turbulence intensities, to see the trend more clearly. In addition, and following Tarald's suggestions in his thesis, it is suggested that future research should include wake measurements to gain a deeper understanding of the complex flow structures surrounding the blades. By examining the wake characteristics, researchers can gather valuable insights into the efficiency and performance of the wind turbine models with swept blades.

References

Ang Li, Georg Raimund Pirrung, Mac Gaunaa, Helge Aagaard Madsen, and Sergio González Horcas. (2022). A computationally efficient engineering aerodynamic model for swept wind turbine blades. *European Academy of Wind Energy eawe*.

Anthony J. Wheeler, Ahmad R. Ganji. (2010). *Introduction to Engineering Experimentation.* Pearson.

Ashwill T, Kanaby G, Jackson K, Zuteck M. (2010). Development of the sweep-twist adaptive rotor (STAR) blade. *Aerospace Sciences Meeting Including the New Horizons Forum and Aerospace Exposition*.

Enel Green Power. (2022, 06 06). *Extending wind blades to maximize power production*. Retrieved from https://openinnovability.enel.com/challenges/call/2022/5/blade-tip-extender-wind-turbines

Energy. (2022). Retrieved from Our World in Data: https://ourworldindata.org/energy

G.M. Joselin Herbert, S. Iniyan, E. Sreevalsan, S. Rajapandian. (2007, 08). *A review of wind energy technologies*. Retrieved from Renewable and Sustainable Energy Reviews: https://www.sciencedirect.com/science/article/abs/pii/S136403210500095X

Hannah Ritchie and Max Roser. (2022). *Energy mix, Our World in Data*. Retrieved from Our World in Data: https://ourworldindata.org/energy-mix

Hannah Ritchie and Max Roser. (2022). *Energy Mix, Our World in Data*. Retrieved from https://ourworldindata.org/energy-mix

Hannah Ritchie, Max Roser and Pablo Rosado. (2022). *Energy, Our World in Data*. Retrieved from https://ourworldindata.org/energy

Hannah Ritchie, Max Roser and Pablo Rosado. (2022). *Renewable Energy, Our World in Data*. Retrieved from https://ourworldindata.org/renewable-energy

J.F. Manwell, J.G. McGowan and A.L. Rogers. (2002). *Wind Energy explained.* Amherst, Massachusetts: Wiley.

Joel Balbien. (2021). Wind Turbines and Computational Fluid Dynamics. *ResearchGate*.

Krogstad P.Å., Lund J.A. (2011). An experimental and numerical study of the performance of a model turbine. *Wind Energy*.

Krogstad PÅ, Adaramola MS. (2011). Performance and near wake measurements of a model horizontal axis wind turbine. *Wind Energy*.

Leon Li, R. Jason Hearst. (2021). The influence of freestream turbulence on the temporal pressure. *Journal of Wind Engineering and Industrial Aerodynamics*.

Liz Hartman. (2022, 08 16). *Wind Turbines: the Bigger, the Better*. Retrieved from Liz Hartman: https://www.energy.gov/eere/articles/wind-turbines-bigger-better

M.S. Adaramola, P.-Å. Krogstad. (2011). Experimental investigation of wake effects on wind turbine performance. *Renewable Energy*.

Mehmet Numan Kaya. (2018). Aerodynamic performance of a horizontal axis wind turbine with forward and backward swept blades.

National Geographic. (2022). *Wind Energy*. Retrieved from https://education.nationalgeographic.org/resource/wind-energy/

Office of Geothermal and Wind Technologies. (2000). *Advanced Airfoils for Wind Turbines.* Retrieved from https://www.nrel.gov/docs/fy00osti/23696.pdf

Samuel Mitchell, Iheanyichukwu Ogbonna and Konstantin Volkov. (2021). Aerodynamic Characteristics of a Single Airfoil for Vertical Axis Wind Turbine Blades and Performance Prediction of Wind Turbines. *MDPI*.

Scott Larwood, C.P. van Dam and Daniel Schow. (2014). Design studies of swept wind turbine blades. *Renewable Energy*.

Sebastian Ehrich, Carl Michael Schwarz, Hamid Rahimi, Bernhard Stoevesandt and Joachim Peinke. (2018). Comparison of the Blade Element Momentum Theory with Computational Fluid Dynamics for Wind Turbine Simulations in Turbulent Inflow. *MDPI*.

Simis. (2023). *Ashes*. Retrieved from https://www.simis.io/

Tarald Wærness. (2021). *An experimental study of the effects of turbulence on the performance of a wind turbine model with forward and backward swept blades.* Trondheim: NTNU.

The Editors of Encyclopaedia Britannica. (n.d.). *Energy*. Retrieved from https://www.britannica.com/science/energy

Universität Oldenburg. (2022). *Active Grid*. Retrieved from https://uol.de/en/twist/research/turbulent-flows/active-grid

Vahid Akbari, Mohammad Naghashzadegan, Ramin Kouhikamali, Farhad Afsharpanah and Wahiba Yaïci. (2022). Multi-Objective Optimization and

Optimal Airfoil Blade Selection for a Small Horizontal-Axis Wind Turbine (HAWT) for Application in Regions with Various Wind Potential. *ResearchGate*, 22.

Xiaoxi Huang, Junwei Yang, Zhiying Gao, Chenglong Sha and Hua Yang . (2022). Output Power and Wake Flow Characteristics of a Wind Turbine with Swept Blades. *MDPI*.

Xiaoxi Huang, Junwei Yang, Zhiying Gao, Chenglong Sha and Hua Yang. (2022). Output Power and Wake Flow Characteristics of a Wind Turbine with Swept Blades. *MDPI*.

Appendices

4.1 Additional results

4.1.1 Reference 9.8 m/s

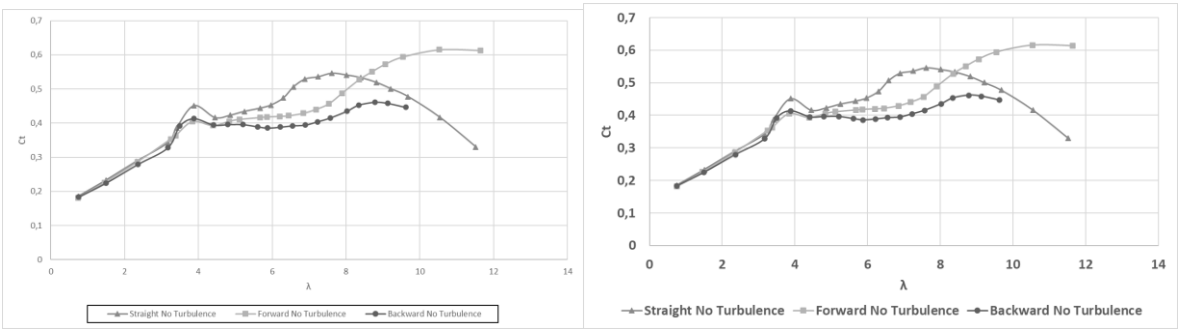

(a) (b)

Figure 41. Effects of blade sweep for the wind turbine models with straight blades, forward swept and backward swept. (a) power coefficients C_p and (b) thrust coefficients C_T at different tip speed ratios, λ. The figure depicts the reference test case, without active grid (Ti = 1 %). The reference velocity was kept constant at U∞ = 9.8 m/s for all the test cases. Thus, the tip speed ratio was only varying with the rotational velocity of the rotors, ω.

4.1.2 Low turbulence 9.8 m/s

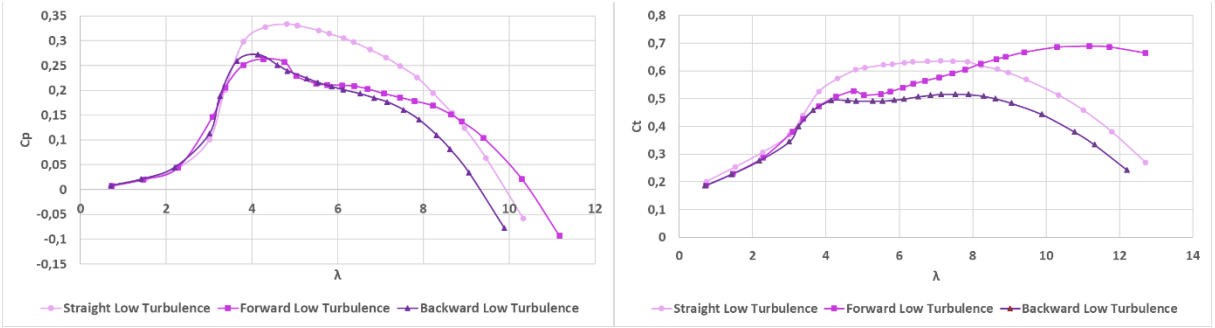

(a) (b)

Figure 42. Effects of blade sweep for the wind turbine models with straight blades, forward swept and backward swept. (a) power coefficients C_p and (b) thrust coefficients C_T at different tip speed ratios, λ. The figure depicts the reference test case, without active grid (Ti = 3 %). The reference velocity was kept constant at U∞ = 9.8 m/s for all the test cases. Thus, the tip speed ratio was only varying with the rotational velocity of the rotors, ω.

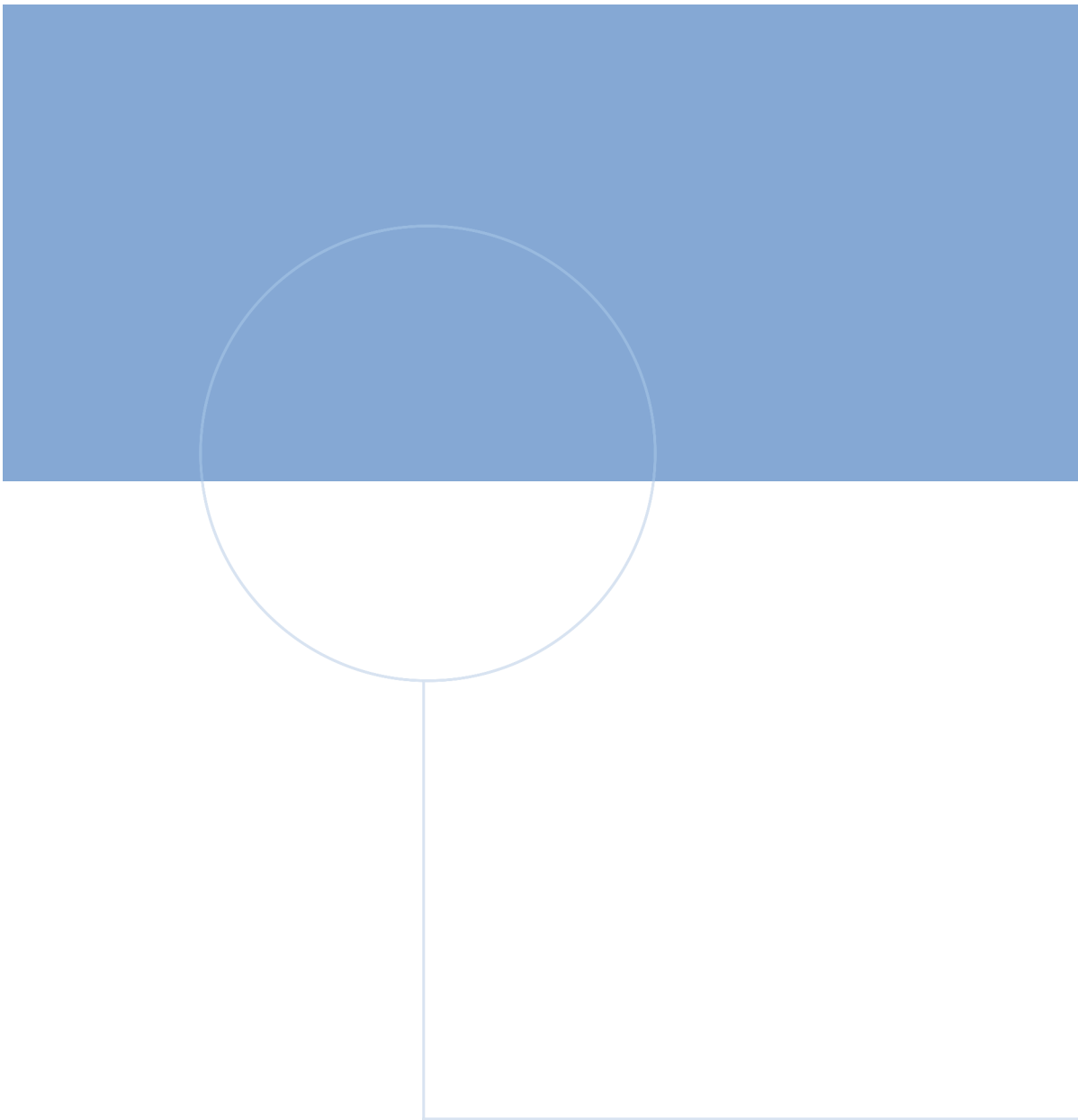

NTNU

Norwegian University of
Science and Technology